

Review

A Review of Thermal Energy Management of Diesel Exhaust after-Treatment Systems Technology and Efficiency Enhancement Approaches

Gang Wu¹, Guoda Feng¹, Yuelin Li¹, Tao Ling², Xuejun Peng², Zhilai Su² and Xiaohuan Zhao^{3,*} 

¹ College of Automotive and Mechanical Engineering, Changsha University of Science and Technology, Changsha 410114, China; wugang@csust.edu.cn (G.W.); fguoda@163.com (G.F.)

² China Railway Wujia Group First Engineering Co., Ltd., Changsha 410114, China; 1071916427@163.com (Z.S.)

³ Energy and Electricity Research Center, International Energy College, Zhuhai Campus, Jinan University, Zhuhai 519070, China

* Correspondence: xiaohuanzhao@jnu.edu.cn

Abstract: The DOC (diesel oxidation catalyst), DPF (diesel particulate filter), SCR (selective catalytic reduction), and ASC (ammonia slip catalyst) are widely used in diesel exhaust after-treatment systems. The thermal management of after-treatment systems using DOC, DPF, SCR, and ASC were investigated to improve the efficiency of these devices. This paper aims to identify the challenges of this topic and seek novel methods to control the temperature. Insulation methods and catalysts decrease the energy required for thermal management, which improves the efficiency of thermal management. Thermal insulation decreases the heat loss of the exhaust gas, which can reduce the after-treatment light-off time. The DOC light-off time was reduced by 75% under adiabatic conditions. A 400 W microwave can heat the DPF to the soot oxidation temperature of 873 K at a regeneration time of 150 s. An SCR burner can decrease NO_x emissions by 93.5%. Electrically heated catalysts can decrease CO, HC, and NO_x emissions by 80%, 80%, and 66%, respectively. Phase-change materials can control the SCR temperature with a two-thirds reduction in NO_x emissions. Pt-Pd application in the catalyst can decrease the CO light-off temperature to 113 °C. Approaches of catalysts can enhance the efficiency of the after-treatment systems and reduce the energy consumption of thermal management.

Keywords: thermal management; diesel exhaust after-treatment systems; heat loss; energy consumption; efficiency of thermal management



Citation: Wu, G.; Feng, G.; Li, Y.; Ling, T.; Peng, X.; Su, Z.; Zhao, X. A Review of Thermal Energy Management of Diesel Exhaust after-Treatment Systems Technology and Efficiency Enhancement Approaches. *Energies* **2024**, *17*, 584. <https://doi.org/10.3390/en17030584>

Academic Editor: Anastassios M. Stamatelos

Received: 22 December 2023

Revised: 21 January 2024

Accepted: 23 January 2024

Published: 25 January 2024



Copyright: © 2024 by the authors. Licensee MDPI, Basel, Switzerland. This article is an open access article distributed under the terms and conditions of the Creative Commons Attribution (CC BY) license (<https://creativecommons.org/licenses/by/4.0/>).

1. Introduction

Due to their efficiency and reliability [1,2], diesel engines are still widely used in transportation for the long term [3,4]. However, the hydrocarbon (HC), carbon monoxide (CO), nitrogen oxides (NO_x), and particulate matter (PM) in the exhaust gas of diesel engines seriously threaten human health [5,6]. Governments have successively introduced emission regulations to limit the emissions of diesel engines [7,8]. To meet the emission regulations, diesel oxidation catalysts (DOCs) [9,10], diesel particulate filters (DPFs) [11,12], and selective catalytic reduction (SCR) [13,14] are widely used in diesel exhaust gas after-treatment systems. However, the efficiency of DOC, SCR, and DPF is closely related to temperature [15,16]. The emission is poor [17,18] at a low exhaust temperature [19,20], and DOC and SCR are at a low efficiency level [21,22]. The urea stops injecting when the temperature is below 200 °C [23,24]. A large amount of HC, CO, and NO_x will be directly discharged into the atmosphere if the exhaust gas is not treated at this time. Due to the low temperature, PM cannot be eliminated, resulting in blockage in the DPF, which deteriorates the performance of the engine [25,26]. The substrate will melt, and the activity of the catalysts will decrease or even fail, if the temperature is too high [27,28].

Therefore, diesel after-treatment thermal management is crucial for the efficiency of the after-treatment system.

Bai et al. [29] reported that a 15–20% opening of the intake throttle valve could increase the exhaust temperature to more than 200 °C, and the NO_x emission under the world harmonized transient cycle (WHTC) could be reduced by 41.5%. They have performed experiments under transient conditions that provide a reference for practical applications. Honardar et al. [30] investigated the effect of post injection timing on exhaust gas temperature and brake-specific fuel consumption (BSFC) on a 1.56 L diesel engine. The exhaust gas temperature increased from 260 °C to 300 °C and the BSFC deteriorated from 530 g/kWh to 620 g/kWh when the post injection timing was postponed from 130 °CA BTDC to –10 °CA BTDC. Brin et al. [31] increased exhaust gas temperature by more than 50 °C with a turbine bypass under the cold federal test procedure (FTP). Turbine bypass might be an optimal thermal management strategy. Salehi et al. [32] optimized the exhaust valve opening (EVO) timing, which reduced the SCR light-off time from 659 s to 500 s, but the fuel consumption increased by 4.1%. Kovacs et al. [33] retarded the intake valve closing timing by 50°, which caused a 20 °C increase in the exhaust temperature and 1.4% reduction in fuel consumption. This research provided a method, intake valve closing timing, that saved fuel and raised the exhaust temperature at the same time.

Hamedi et al. [34] investigated a double-layer exhaust pipe thermal insulation strategy via CFD. The result showed that the DOC inlet temperature increased by 12 °C and the emissions of CO and HC were both reduced by 17%. Burch et al. [35] led to a 52% and 29% reduction in total CO and HC emissions, respectively, via vacuum insulation and phase-change materials (PCMs). Excellent results have been obtained by combining phase-change materials and thermal insulation. Feng et al. [36] increased the SCR inlet temperature by 19.9 °C on average, and improved the NO_x conversion efficiency up to 8.0%, with an electrically heated catalyst (EHC). Miao et al. [37] employed a 4.85 kW EH-SCR and a 5.4 kW EH-DOC to shorten the SCR light-off time by 62 s. The dual EHC system presented in that study significantly reduced SCR light-off time. Ma et al. [38] developed an afterburner to reduce the catalytic converter light-off time to below 20 s. Sharp et al. [39] studied the influence of the mini-burner on exhaust gas temperature and fuel consumption. The results showed that SCR reached 200 °C at around 200 s, 400 s faster than baseline, but the fuel consumption increased by 2.6%. They used the burner for SCR and significantly reduced the light-off time. Kurien et al. [40] reported that the DPF with a 400 W microwave achieved a soot light-off temperature of 873 K at a regeneration time of 150 s.

Various methods of diesel engine after-treatment thermal management are listed in this paper. The feature of the study is a focus on non-engine-based after-treatment thermal management technologies, describing thermal management control strategies in detail and summarizing the effects of the various thermal management strategies on exhaust temperature, emission concentrations, and fuel consumption. Some catalysts that help with thermal management are also mentioned. A summary of the relevant literature as well as an identification of deficiencies and challenges are both presented in this paper.

2. Composition and Work Principle of Diesel Engine after-Treatment Systems

As shown in Figure 1, a typical diesel after-treatment system consists of a DOC, DPF, SCR, and ASC (ammonia slip catalyst) [41].

2.1. DOC

The DOC is the first after-treatment device through which exhaust gas flows [42]. The working principle of the DOC is to oxidize the CO and HC in the exhaust gas [43,44]. The DOC also oxidizes NO to NO₂ [45], which increases the ratio of NO₂ in NO_x. A high ratio of NO₂ assists DPF regeneration [46] and improves NO_x conversion in SCR [47]. The heat released by the oxidation reaction in the DOC increases the downstream temperature, which assists the DPF light-off [48]. The DOC consists of the shell, the shock-absorbing

layer, the substrate, and the catalyst coating [49] (Figure 2a). The substrate of the DOC is a flow-through monolith with a catalyst coating [50] (Figure 2b).

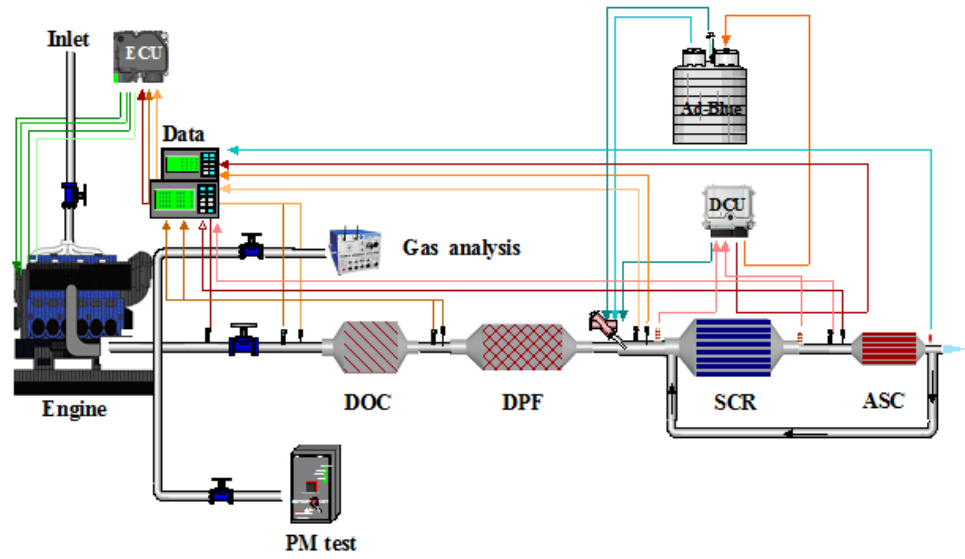


Figure 1. Architecture of diesel engine exhaust after-treatment system.

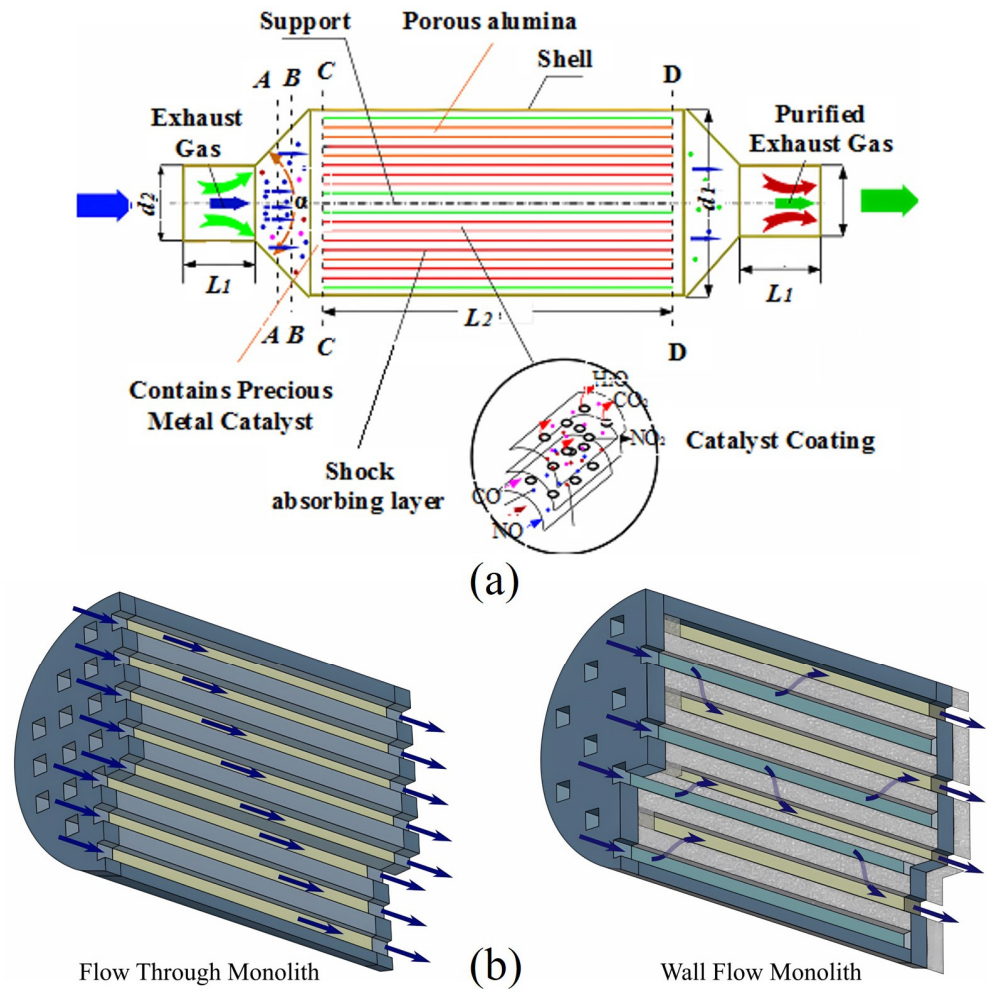
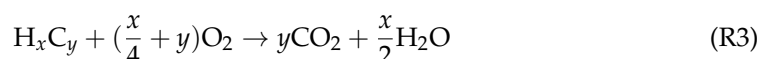


Figure 2. Structure diagram of catalyst carrier. (a) Schematic diagram of DOC structure [49]. (b) The structures of a flow-through monolith and a wall-flow monolith [50].

The active components in the catalyst reduce the reaction activation energy and promote the oxidation reactions of CO, HC, and NO [51]. CO, H_xC_y (=HC) and NO enter the DOC, are adsorbed onto the catalyst coating, and react with CO_2 , NO_2 , and H_2O as follows (reactions (R1)–(R3)) [52]:

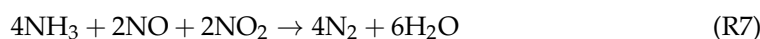
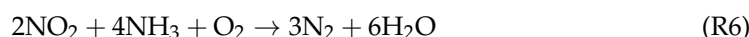


2.2. DPF

The exhaust gas flows through the wall of the DPF, and then the PM is filtered, which is the working principle of the DPF [53]. The substrate of the wall-flow DPF has a wall-flow monolith, in that the ends of the channels in it are alternately plugged [50] (Figure 3a). The accumulation of PM leads to a back-pressure increase, which leads to a deterioration of the engine performance [54]. The process of removing PM is DPF regeneration. DPF regeneration is classified as active regeneration and passive regeneration [55,56]. Efficient oxidation of PM requires a certain high temperature [57]. Active regeneration is a method that actively injects energy to increase the DPF temperature to the soot light-off temperature. For example, engine-based heating measures [58,59] or microwave-regeneration-based [60,61] active regeneration include post injection in the DOC [62,63] and an extra heating device [64,65]. Passive regeneration includes NO_2 oxidation-assisted regeneration [66,67], catalytic diesel particulate filters, (CDPFs) (Figure 3b) [68,69], etc., but requires no energy input. A lot of heat is released during the regeneration (Figure 3c) [70,71], which causes the DPF to age and deteriorates the efficiency of SCR at the downstream side of the DPF [72,73]. Therefore, thermal management is important during regeneration.

2.3. SCR and ASC

The role of SCR is to reduce NO_x to nitrogen (N_2) [27]. The exhaust gas contacts the reducing agent in the SCR, and the reducing agent catalytically reduces NO_x to N_2 (as shown in Figure 4). For reasons of safety and toxicity, an aqueous solution of urea (NH_2CONH_2) is the preferred selective reducing agent for SCR [76]. NH_3 is produced via the hydrolysis of urea injected (reaction (R4)) by the urea solution injector upstream of the SCR [76]. The ASC is installed at the downstream side of the SCR and is used to react the unreacted NH_3 [77,78]. The main reactions in SCR and ASC are as follows (reactions (R5)–(R13)) [79,80].



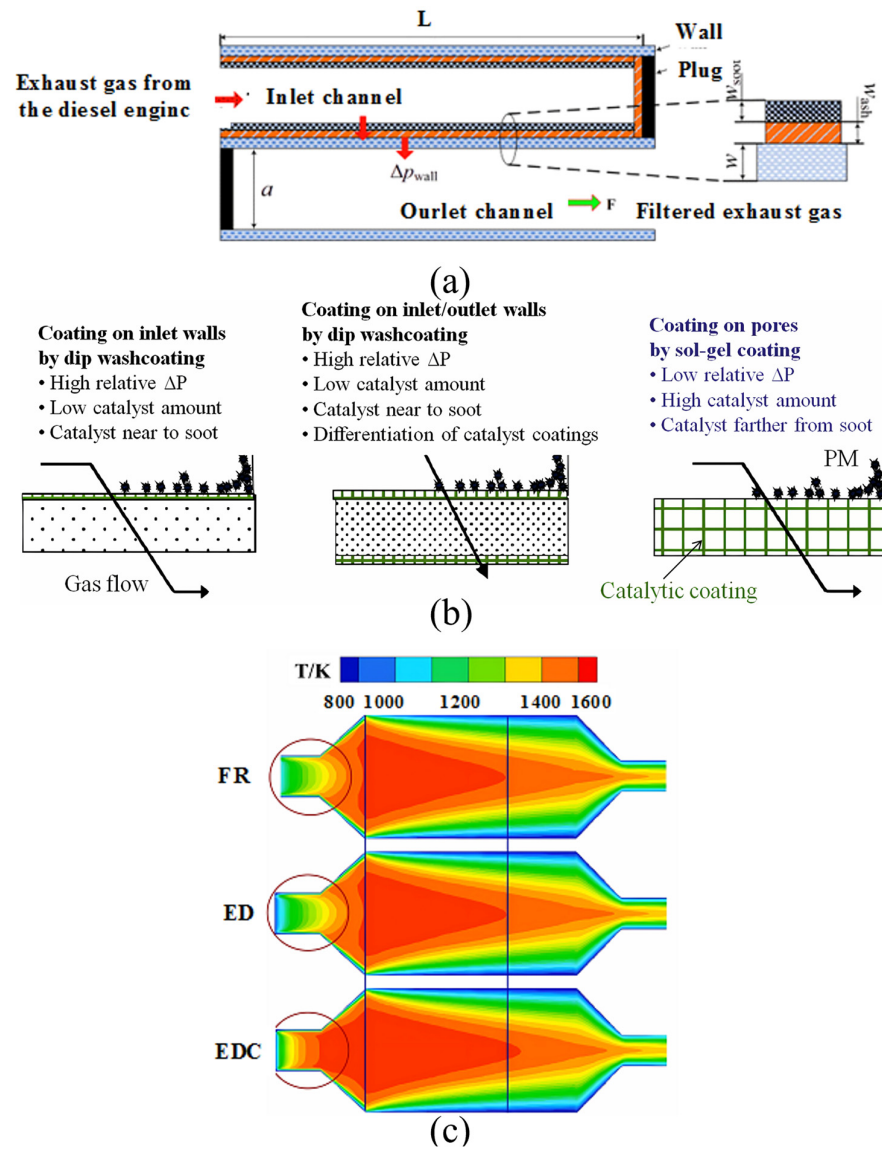


Figure 3. Schematic of the DPF. (a) Side view of adjacent channels [74]. (b) Methods for catalytic coatings on the DPF [75]. (c) Temperature contour of soot combustion reaction [71].

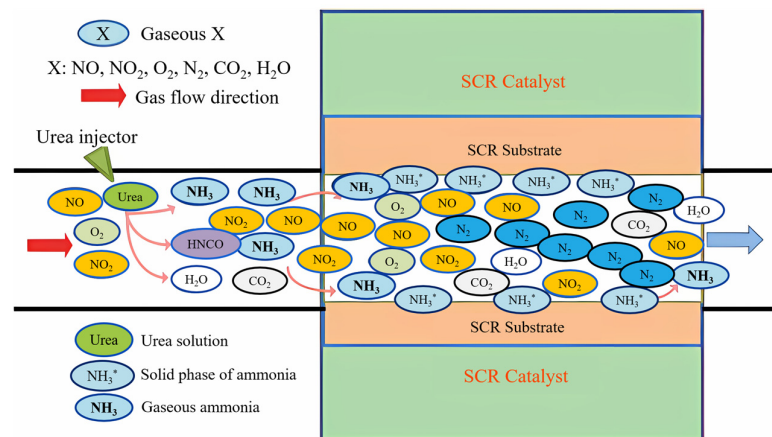


Figure 4. Principle illustration of urea-based SCR diesel engine after-treatment system [81].

3. After-Treatment Thermal Management Technology

3.1. Exhaust Gas Thermal Management

The high initial exhaust gas temperature can accelerate the after-treatment system to ignite without other heating devices. Taking the DOC as an example, achieving an increase in the initial exhaust temperature under low exhaust temperature conditions helps the DOC to start oxidizing CO and HC earlier, and the exothermic oxidation reaction further increases the temperature. As the engine load gradually increases, the exhaust gas temperature also increases further. Thus, the DOC ignites earlier. The effects of engine control technologies such as variable valve timing technology (VVT) [82,83], injection technology [84], variable geometry turbo technology (VGT) [85], etc. on the exhaust temperature, BSFC, and BTE are listed in Table 1. EEVO, intake throttle, exhaust throttle, and post injection technology can raise the exhaust temperature and reduce the thermal efficiency. VGT and IVC may be the ways to improve thermal efficiency and exhaust gas temperature and effectively solve the trade-off problem between thermal efficiency and exhaust gas temperature. Injection timing slightly affects the exhaust temperature but reduces the BSFC.

Table 1. Increase or decrease in exhaust temperature, BTE, and BSFC via different thermal management methods.

Thermal Management Methods	Test Conditions	Increase in Exhaust Temperature	Effect on BTE or BSFC	
			BTE	BSFC
EEVO [82]	Low-load	90 °C	↓5%	N.A.
IVC [83]	1200 rpm, 2.5 bar	65 °C	N.A.	↑9.3%
Injection timing [84]	1100 rpm, 100 N·m	28 °C	N.A.	↓17 g/(kW·h)
Intake throttle [85]	1300 rpm, 0.4 Mpa	38 °C	↓0.75%	N.A.
Exhaust throttle [85]	1300 rpm, 0.4 Mpa	60 °C	↓1.95%	N.A.
Post injection technology [85]	1300 rpm, 0.4 Mpa	57 °C	↓3%	N.A.
VGT [85]	1300 rpm, 0.4 Mpa	50 °C	↑7%	N.A.

VVT is a technology that can adjust the open and close timing of the intake and exhaust valves based on engine operating conditions to run the engine in an optimized state [86,87]. Employing VVT also increases the exhaust gas temperature. Robert et al. [82] used a model to predict the effect of early exhaust valve opening (EEVO) on the exhaust gas temperature under a low load condition. The model predicted an approximate 30 °C–100 °C increase in turbine out temperature and a 5% reduction in BTE when the EVO was 90° before nominal. Basaran et al. [83] investigated the effect of early intake valve closing (EIVC) and late intake valve closing (LIVC) on exhaust temperatures. The result showed that both EIVC and LIVC increase the exhaust temperature. The exhaust temperature was higher than 250 °C when the valve timing was earlier than −25 °CA ATDC or later than 115 °CA ATDC. Fuel injection timing affects the heat release rate, and thus, it is related to exhaust temperature and engine thermal efficiency. Bai et al. [84] studied the impacts of the injection advance angle on exhaust temperature and fuel consumption through experiments. When the injection advance angle was postponed from −4 °CA to 7 °CA, the exhaust temperature increased from 225 °C to 253 °C, and the fuel consumption increased by 17 g/(kWh) at a condition of 1300 r/min and 300 N·m. In general, the main injection timing has little effect on exhaust temperature and fuel consumption. The results of the above papers were obtained under steady-state conditions and present us with the thermal management effect of VVT technology, but further transient experiments are needed for practical application.

To find ways to improve thermal efficiency and increase exhaust temperature, Wu et al. [85] studied the influence of intake throttle, exhaust throttle, post injection, and VGT on exhaust temperature and BTE. The exhaust gas temperature increased by 40 °C and 60 °C, and the BTE decreased by 1% and 2%, respectively, when the opening of the intake throttle valve and the exhaust throttle valve were sufficiently reduced (Figure 5a,b). The parameters of the post injection quantity and timing had significant effects on the exhaust

temperature and thermal efficiency. When the timing was retarded from 30 °CA ATDC to 70 °CA ATDC, the exhaust temperature increased by 50 °C, and the BTE decreased by about 1% at a constant post injection quantity of 9 mg. When the post injection quantity increased from 3 mg to 15 mg, exhaust temperature increased by 50 °C, but the BTE decreased by 3% (Figure 5c,d). As shown in Figure 5e,f, the exhaust temperature increased by about 50 °C and the BTE increased by about 7% with the reduction in the VGT working capacity.

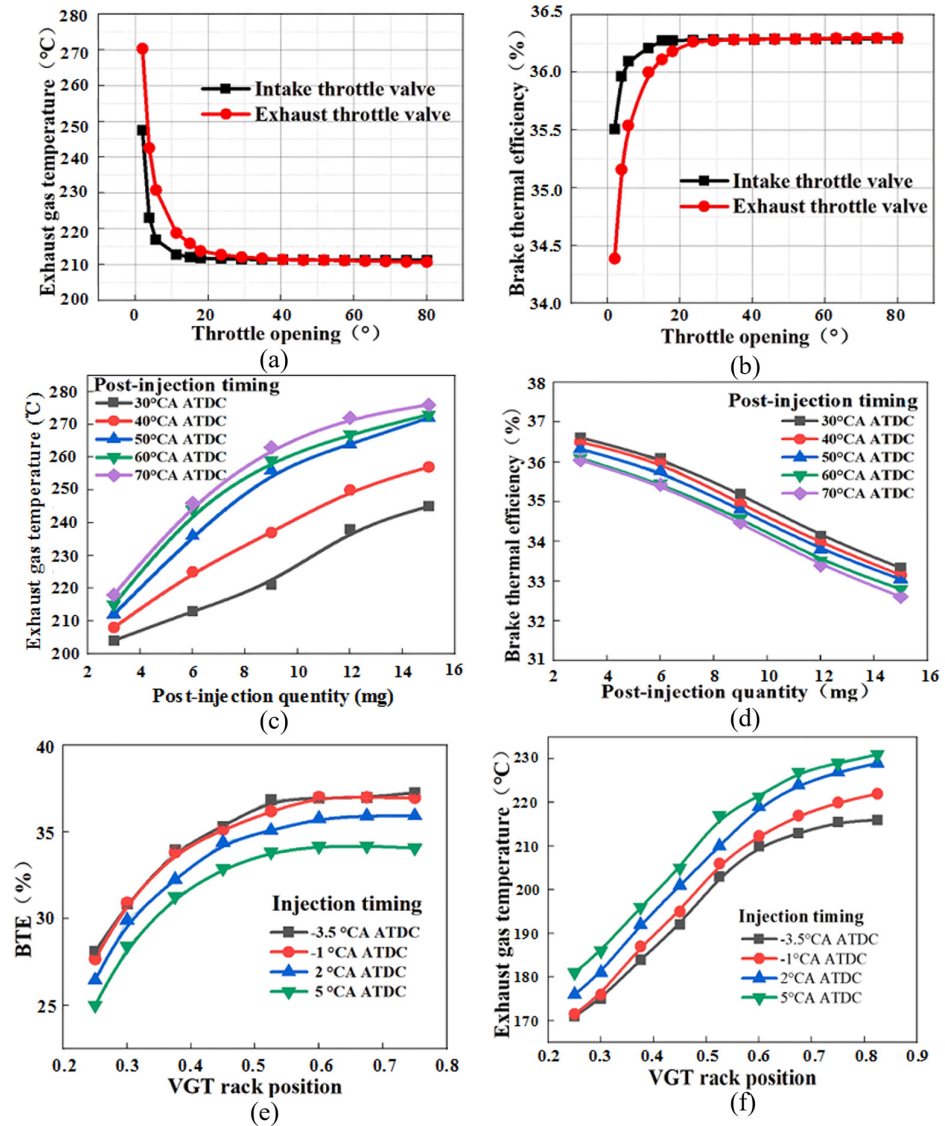


Figure 5. Effects of different thermal management techniques on exhaust gas temperature and BTE [85]. (a) Relationship between throttle opening and exhaust gas temperature. (b) Relationship between throttle opening and BTE. (c) Effect of post injection on exhaust gas temperature. (d) Effect of post injection on BTE. (e) Effect of VGT on exhaust gas temperature. (f) Effect of VGT on BTE.

3.2. DOC Thermal Management

The conversion efficiency of the DOC is closely related to temperature because the catalytic activity of catalysts is positively correlated with temperature. Take the common Pt precious metal catalyst as an example. CO conversion reached 100% at a temperature of around 180 °C, while HC conversion reached 40% at a temperature of 270 °C [88]. Ho et al. [89] presented that CO conversion and C₃H₆ conversion reached 100% at a temperature of around 300 °C, but when the temperature was 150 °C, the CO conversion and C₃H₆ conversion were 20% and 0%, respectively. A lot of CO and HC will be released into the atmosphere without being treated at low temperatures. Therefore, rapid DOC

light-off is crucial [90,91]. High-temperature exhaust gas has a significant effect on DOC light-off. As shown in Figure 6a, Grag et al. [92] increased the exhaust temperature from 195 °C to 255 °C by adjusting the intake valve closing timing. Chuan et al. [93] increased the exhaust temperature from 190 °C to 310 °C, which was higher than the DOC light-off temperature, via cylinder deactivation (CDA) at idle operation. Neely et al. [94] applied intake throttle technology to raise the turbocharger outlet temperature to 230 °C at the condition of 1200 rpm, 1.7 bar BMEP, and 25 °C coolant temperature. Francisco et al. [95] explored exhaust pipe thermal insulation to increase the DOC inlet temperature and accelerate DOC light-off. The adiabatic exhaust port (EP), exhaust manifold (EM), internal surface of the turbine volute (TI), and turbine external housing were simulated under the WTLC. The result is shown in Figure 6b. DOC light-off took 800 s without any insulation, while DOC light-off took only about 200 s when all parts were completely insulated. The exhaust manifold was the part that lost the most heat. The rapid DOC light-off also benefits from external heat sources such as burners and EHCs.

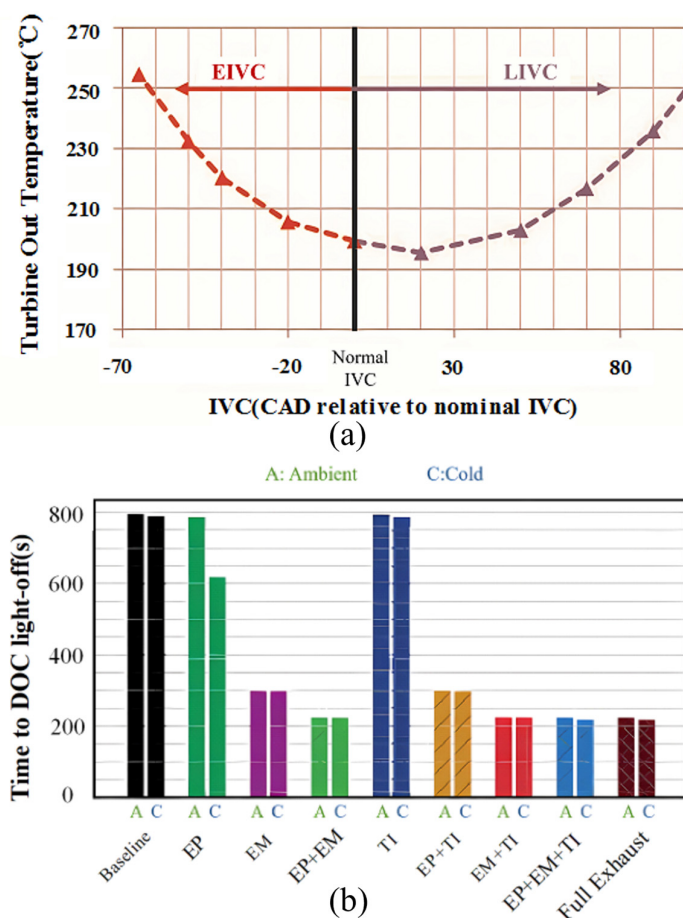


Figure 6. Data of exhaust temperature and DOC light-off time. (a) Exhaust gas temperatures along EIVC and LIVC sweeps at 1200 RPM, 2.5 bar BMEP [92]. (b) Time to reach the DOC light-off temperature [95].

Zhao et al. [96] added a burner upstream of the DOC. The simulation calculation showed that it took 65 s for the 1.54 kg DOC substrate to reach a temperature of 300 °C at the condition of 79.2 kg/h exhaust flow rate and 25 °C initial temperature. In practical situations, the actual light-off time will increase due to the interference of factors such as heat transfer loss. Paolo et al. [97] employed an EHC to heat the DOC. The DOC employing EHC took about 220 s to reach the peak temperature in driving cycle conditions, and the temperature of the DOC could be maintained at more than 50% of the peak temperature through the on-off control of the electric heater.

3.3. DPF Thermal Management

The soot oxidation light-off temperature of the DPF is higher than the DOC light-off temperature [98,99]. Under the normal operation of diesel vehicles, the exhaust temperature (200–400 °C) cannot meet the continuous oxidation of O₂/NO₂ to the accumulated PM [100]. Even if the catalyst is applied, high temperatures are required. When the Printex-U load of 3.5 g/L was regenerated at 400 °C, the filtration efficiency of particles showed a value of 86.4% [101]. Tan et al. [102] increased the DOC outlet temperature to 550 °C via a late post injection technology, but raising the DPF inlet temperature in that way was accompanied by worsening fuel consumption [103]. The diesel vaporizer system was to introduce diesel into the DOC to intensify the oxidation heat release of the DOC [104], which enabled the DOC outlet temperature to reach 650 °C rapidly, with a fuel consumption reduction of 50%. Utilizing the HC tailpipe injection could reduce extra fuel consumption. The injection amount is calculated according to the target temperature via Equation (1). This formula is idealized, and its premise is that all fuel is fully oxidized by the DOC to heat the exhaust gas [105]:

$$\dot{m}_{\text{fuel}} = \dot{m}_{\text{exhaust}} \times \Delta T_{\text{exhaust}} \times \frac{c_p}{H} \quad (1)$$

where \dot{m}_{fuel} is the mass flow rate of fuel injection, kg/h; \dot{m}_{exhaust} is the mass flow rate of the exhaust gas, kg/h; c_p is the specific heat of the exhaust gas, kJ/kg/K; $\Delta T_{\text{exhaust}}$ is the difference between the target exhaust temperature and the incoming exhaust temperature, K; and H is the lower heating value of the diesel fuel, kJ/kg.

Microwaves rapidly heat the DPF to the soot light-off temperature. Kurien et al. [106] utilized microwaves to raise the maximum temperature of the substrate to 800 K and the average temperature to more than 600 K in a regeneration time of 180 s. In [40], the magnetron port power was considered. The DPF reached a soot oxidation temperature of 873 K in a regeneration time of 150 s with a power of 400 W. To minimize microwave energy consumption during DPF regeneration, E et al. [107] developed a microwave energy consumption optimization model and obtained an optimized microwave regeneration power and regeneration heating time. The microwave energy consumption of the four cases was reduced by 5.65%, 5.7%, 10.64%, and 14.64%, respectively. E et al. [108,109] optimized the rotary microwave regeneration performance and obtained a series of optimized regeneration parameter ranges. The optimal parameter ranges of the exhaust temperature, oxygen content, soot mass fraction, and microwave power were 600–750 K, 0.11–1.15, 0.06–0.08, and 800–1200 W, respectively.

Zhao et al. [110] proposed that the field synergy angle could be an index to optimize the temperature distribution of the DPF. Deng et al. [111] concluded that 20–30 g/s was the optimal exhaust mass flow range based on an analysis of the synergy between the vector field and the temperature gradient. Furthermore, wall melting and thermal stress damage could be avoided when the PM load was less than 5 g/L. As shown in Equation (2), the concept of a temperature uniformity coefficient was proposed [112]. The temperature uniformity coefficient describes the temperature distribution of the DPF more accurately. They found that an inlet velocity of 36 m/s and an inlet pressure of 0.08 Mpa were the optimal parameter values based on the formula.

$$R_{TU} = \sqrt{\frac{1}{n} \sum_{j=1}^n \left(\frac{T_j - \bar{T}}{\bar{T}} \right)^2} \quad (2)$$

where T_j is the temperature of a position in the wall-flow filter, K; \bar{T} is the wall-flow filter's average temperature under a certain condition, K; and R_{TU} is the temperature uniformity coefficient.

Drop to idle (DTI) is a driving behavior in which the engine rapidly changes from a high-speed condition to an idle condition. The increase in oxygen content and the decrease in exhaust flow lead to an accumulation of heat in the DPF; thus, the temperature rises

rapidly during DTI [113,114]. The peak temperature and temperature gradient are a concern. The substrate will crack and melt if the temperature gradient and the peak temperature are too high [115,116]. Wang et al. [117] increased the idle speed via EGR and intake throttling to reduce the oxygen concentration in the exhaust gas, which alleviated the intensity of the oxidation reaction. The presence of EGR and intake throttling reduced the peak temperature by 130 °C at an idle speed of 2200 rpm. Bai et al. [118] raised the idle speed from 700 rpm to 1100 rpm, which resulted in a decrease in the peak temperature from 820 °C to 632 °C and a reduction in the maximum temperature gradient from 30 °C/cm to 10 °C/cm. Tan et al. [119] investigated the effect of PM load, target regeneration temperature, and exhaust mass flow on DPF temperature distribution during DTI. The peak temperature and the maximum temperature gradient of the DPF increased by 17% and 48.6%, respectively, when the PM load was increased from 3.6 g/L to 5.6 h/L (Figure 7a). The increase in the target regeneration temperature from 575 °C to 625 °C was accompanied by a 10.5% increase in the peak temperature and a 15.9% increase in the maximum temperature gradient (Figure 7b). When the exhaust mass flow was increased from 40 g/s to 60 g/s, the peak temperature and the maximum temperature gradient were reduced by 7.75% and 48.17%, respectively (Figure 7c).

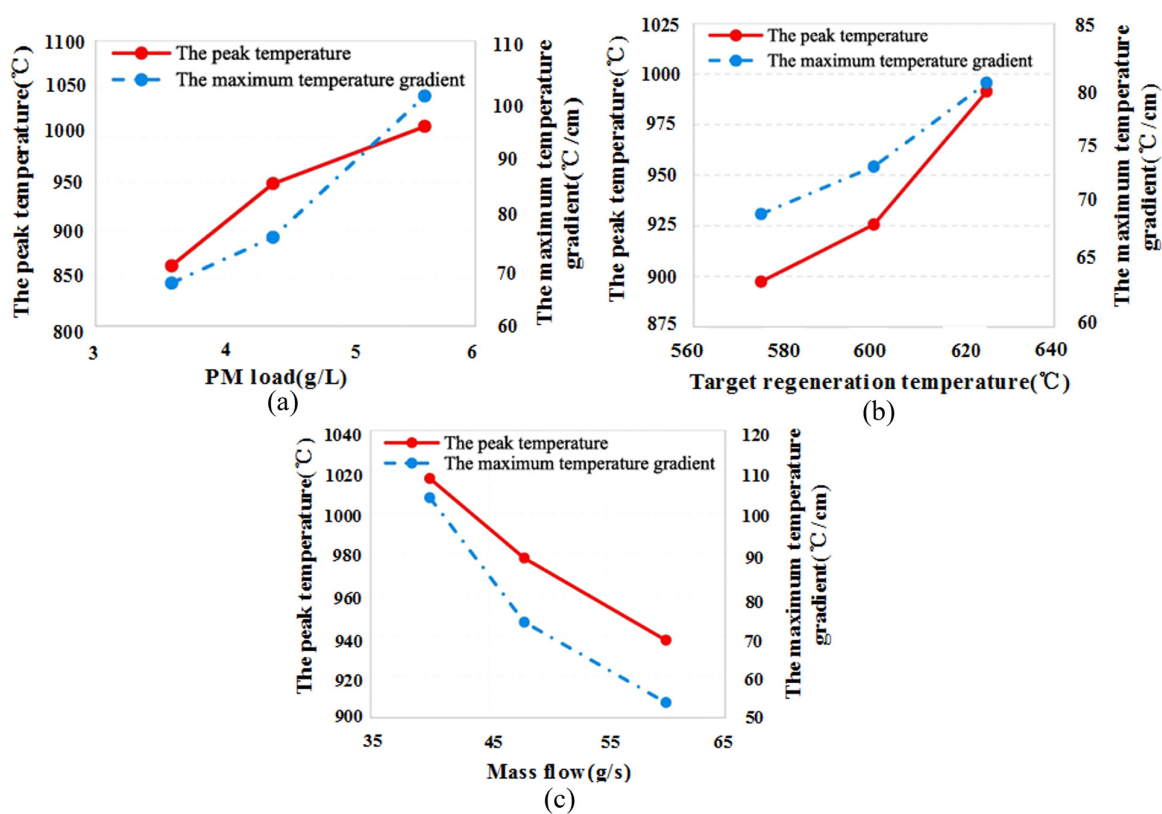


Figure 7. Peak temperature and maximum temperature gradient [119]. (a) The peak temperature and maximum temperature gradient at different PM loads. (b) The peak temperature and maximum temperature gradient at different target regeneration temperatures. (c) The peak temperature and maximum temperature gradient at different mass flows.

3.4. SCR Thermal Management

The catalyst in SCR requires a certain temperature range. An iron titanate catalyst showed good activity in a temperature window of 200–350 °C with the NO_x conversion above 90% [120]. Nicolo et al. [121] adopted a strategy of VGT and fuel injection timing to advance SCR light-off by 600 s under the cold NEDC for the Euro 6 emission regulations. The fuel consumption of SCR increased by 7.39%. Sung et al. [122] proposed a plasma burner to heat the SCR during cold start conditions (Figure 8a). The SCR surface reached

the light-off temperature of 200 °C in only 25 s with the 250 W plasma burner heated. Culbertson et al. [123] studied the impacts of different heating powers on SCR light-off time. SCR reached 200 °C at around 130 s via a 30 kW EHC under the cold FTP, more than 8 min faster than the No EHC case. The catalysts in the SCR have a high conversion efficiency within a specific temperature window [124,125]. SCR will hydrothermally age if exposed to high temperatures for a long time [126,127]. Therefore, the peak temperature of the SCR also needs to be considered. It can be solved using a logic block that was adopted to control the open and close of the burner in [128]. The burner turned off when the maximum set temperature was reached and turned on when it fell below the minimum set temperature. As shown in Figure 8b, the exhaust temperature rose rapidly to 250 °C, and the SCR inlet temperature fluctuated between 200 °C and 250 °C. This indicates that the burner heated up faster and its temperature was relatively stable.

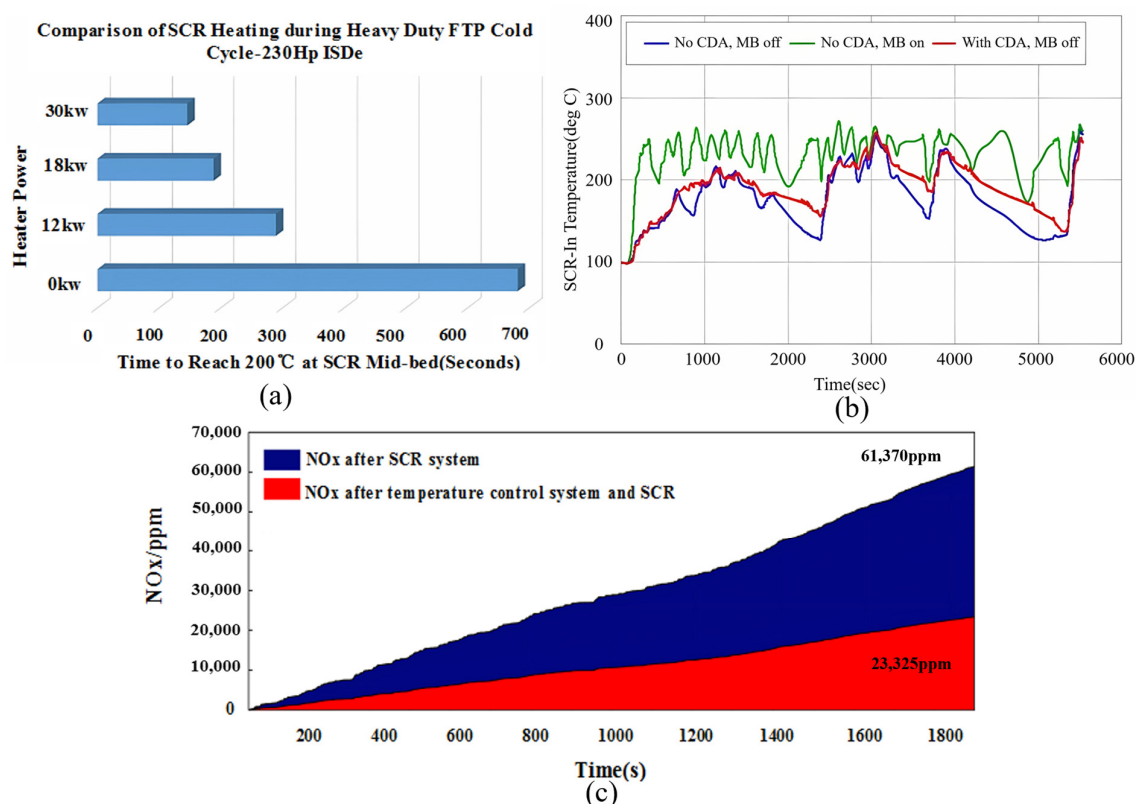


Figure 8. Figures and data of SCR thermal management. (a) Comparison of times to heat SCR mid-bed to 200 °C [122]. (b) SCR inlet temperature data [128]. (c) The total quantity of NO_x elimination with an SCR system only and with an SCR system assisted by a temperature control system [129].

Jiang et al. [129] adopted a PCM to control the temperature of the SCR. After completing the preheating procedure in the European transient cycling (ETC) with a target temperature of 563 K, the fluctuation in the exhaust gas temperature was limited within 30 K. The NO_x conversion efficiency was over 90%, and the total NO_x emission was reduced by about 2/3 (Figure 8c).

4. After-Treatment Systems Efficiency Enhancement Approaches

4.1. Burner

The burners installed at the upstream side of the catalysts heat the exhaust gas directly, which can effectively reduce the light-off time of the DOC. Alexander et al. [130] employed a burner in a 2 L engine after-treatment system. The emission of HC improved significantly when the preheat time was 0.5 s. When the preheat time was extended to about 20 s, the catalytic converter reached the light-off temperature before the engine turned on. Thomas

et al. [131] added a microburner to the engine model. The burner turned on at 4 s under the cold FTP and worked at a constant fuel rate of 0.256 g/s until the end of the cycle. As shown in Figure 9a, the DOC inlet temperature reached 250 °C at 100 s. The late start of the ammonia spray is a limitation.

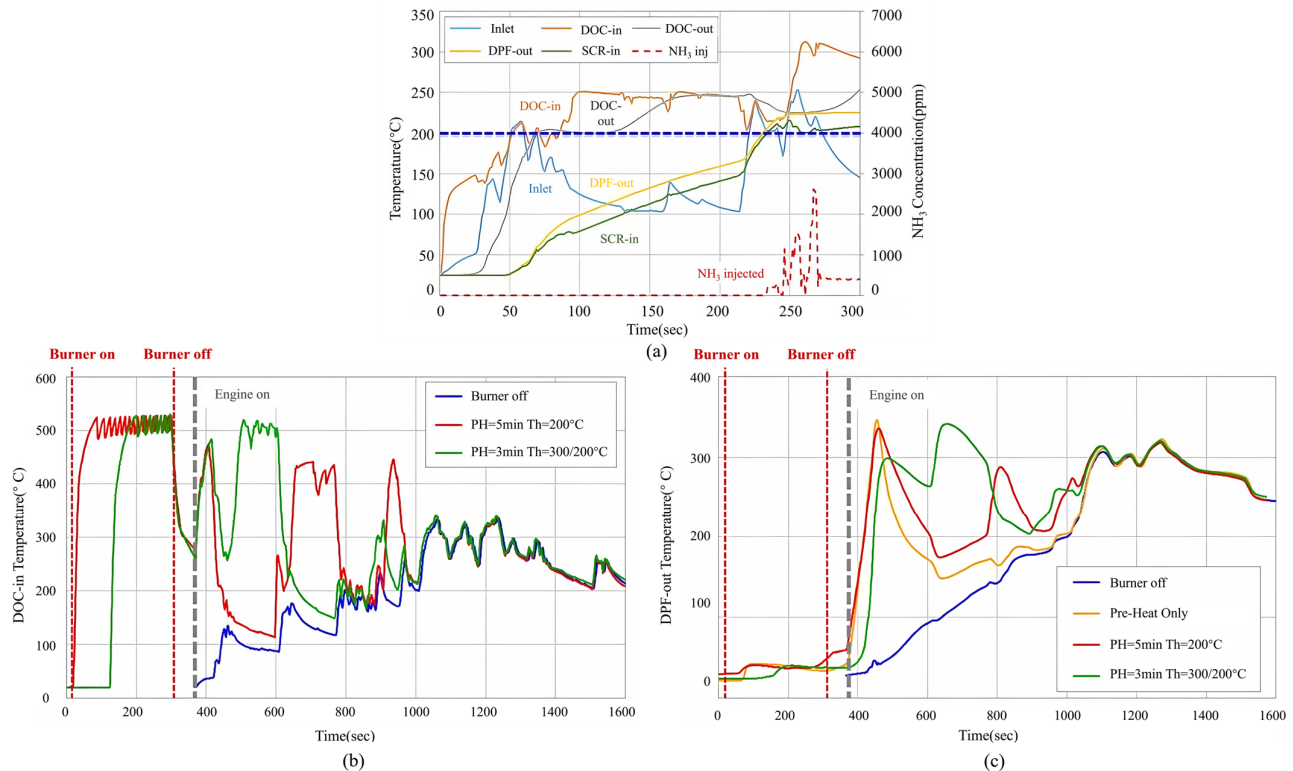


Figure 9. Exhaust gas temperature during preheating and the cold-start FTP cycle. (a) Exhaust gas temperatures at various locations within an after-treatment system that includes an in-exhaust burner [131]. (b) DOC-in temperature during preheating and the cold-start FTP cycle [132]. (c) DPF-out temperature during preheating and the cold-start FTP cycle [132].

Two burner control strategies were proposed in [132], as shown in Figure 9b,c. The control strategy represented by the red line was preheating for 5 min after the engine turned on. The DPF outlet temperature was 200 °C as the threshold temperature. (The burner turned off once the temperature was reached.) The control strategy represented by the green line was preheating for 3 min after the engine turned on, which adopted 300 °C as the threshold temperature once, and then reduced the threshold temperature to 200 °C. The DOC and SCR light-off times were less than 50 s and 100 s, respectively, but the DOC temperature could not be maintained above 250 °C all the time. McCarthy et al. [133] utilized an identical two-tier control strategy for SCR. The SCR inlet temperature was maintained at more than 200 °C, and the emission of NO_x decreased by 93.5%, but the CO₂ emission increased by 9%.

4.2. EHC

EHC is an effective way to improve the efficiency of after-treatment systems. Augusto et al. [134] indicated that nonuniform distribution of the heat generated by the electrical heating device determined the formation of some hot spots inside the catalyst, which promoted the light-off of the reactions at the early cold start condition. Johannes et al. [135] adopted EHC in a hybrid vehicle, which significantly reduced NO_x emission levels during urban and short-distance driving. Pfahl et al. [136] utilized a 1 kW EHC to warm up the DOC under the NEDC. An EHC decreased the DOC light-off time by 100 s, while the conversion rates of HC and CO increased by 20% and 60%, respectively. Pace et al. [137]

reported that 60% less energy was required for the EHC to reach temperature levels similar to engine-based catalyst heating methods.

The EHC is a flexible device. Reasonable control strategies can optimize energy consumption, exhaust temperature, catalyst efficiency, and thermal damage to the catalyst. Gao et al. [138] presented two EHC control strategies and investigated their influence on energy consumption and emissions. As displayed in Figure 10a,b, strategy A meant that the EHC turned off when the engine stopped injecting fuel or the exhaust temperature was higher than the target temperature (T_{target}). Strategy B was that the EHC turned off only when the exhaust gas temperature was higher than the target temperature (T_{target1}) and when the engine stopped injecting fuel. A T_{target2} less than or equal to T_{target1} was set.

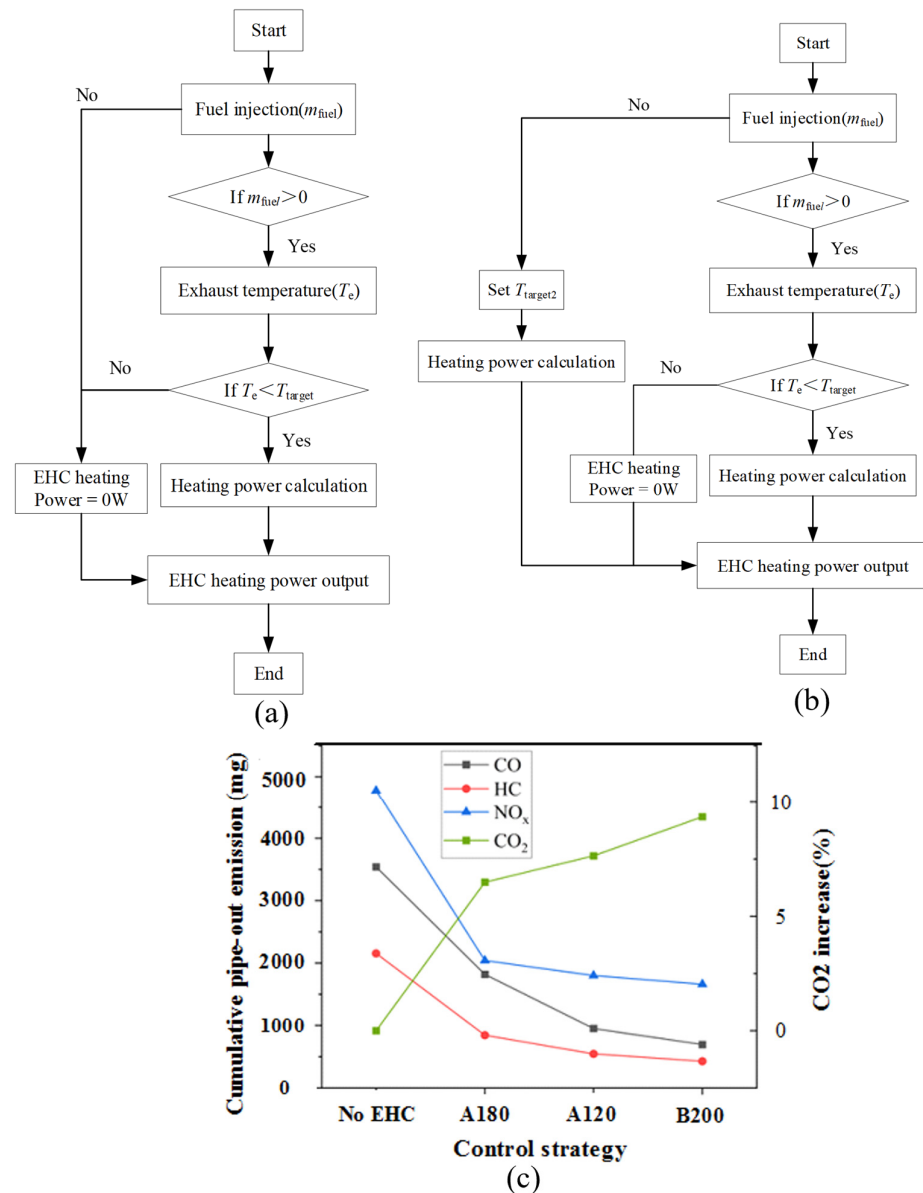


Figure 10. Two different EHC control strategies and a graph of emission data [138]. (a) Control strategy A. (b) Control strategy B. (c) Impact of control strategies on emissions.

Strategy A significantly shortened the catalyst light-off time under the cold WLTC. The light-off times were 254 s and 256 s when the target temperature was set to 180 °C and 200 °C (A180 and A200), respectively. Compared with A180, A200 deteriorated the CO₂ emission by about 18%, and reduced the CO, HC, and NO_x emissions by about 48%, 35%, and 12%, respectively. Compared with the No EHC case, A200 decreased CO, HC,

and NO_x emissions by about 73%, 75%, and 62%, respectively, while the CO₂ emissions increased by 7.64%. In strategy B, when T_{target1} and T_{target2} were both set to 200 °C (B200), the CO, HC, and NO_x emissions were reduced by about 80%, 80%, and 66%, respectively, while the CO₂ increased by 9.35% (as given in Figure 10c). In [139], a pulsating heating strategy with a pulse width of 30 s led to an approximate 70% and 24% reduction in the CO and HC emissions, respectively, under the NEDC. Compared with the typical heating strategy, the pulsating heating strategy increased the CO and HC conversion efficiency by 34% and 31%, respectively. NO_x conversion was much lower than that of CO and HC due to the fact that SCR occurs at the end of the after-treatment system and hardly benefits from the heat of the EHC.

Before the engine is turned on, there is no airflow in the exhaust pipe; therefore, when the preheating strategy was adopted, the heat distribution in the after-treatment devices was uneven, and the downstream devices were insufficiently heated. To solve this problem, Bargman et al. [140] installed an air pump upstream of the after-treatment system and utilized the airflow to preheat the downstream after-treatment devices. The results showed that the emission of NO_x was reduced by 51% in non-methane organic gas under the cold start condition. Hamedi et al. [139] proposed the method of combining EHC with post injection technology, which reduced the total emission of HC by 79% compared with employing the post injection technology individually. Kim et al. [141] combined EHC and HC injection. The 4.8 kW peak power was applied from the start-up, and then, an appropriate amount of HC injection was applied after 20 s when the EHC temperature reached 250 °C. SCR light-off time was within 100 s. Furthermore, the conversion efficiency of the SCR reached 90% during 100 s to 350 s during the cold FTP75. Matheaus et al. [142] studied the effects of EH combined with CDA on SCR emissions reduction and fuel consumption. Compared with CDA individually, EH (5 kW constant) combined with CDA decreased NO_x emissions by 62.5%, and BSFC was increased by 5.7% under the cold FTP. Compared with EH alone, NO_x emissions and BSFC decreased by 50% and 2%, respectively.

The coupling system of a thermoelectric generator and exhaust gas heater was investigated in [143]. Electric energy was generated by the temperature difference between the exhaust gas and cooling water to compensate for the energy consumption of the electric heater through the coupling system. Ximinis et al. [144] implemented a thermoelectric generator and EH coupling system in the after-treatment system of a diesel engine (Figure 11a). Employing a 5 kW EH powered by a thermoelectric generator alone, they were able to increase the SCR conversion efficiency by 55%.

4.3. Thermal Insulation

Thermal insulation improves catalyst performance by reducing exhaust heat loss during engine warm-up. Broatch et al. [145] simulated the effects of exhaust ports and exhaust manifolds under adiabatic conditions on engine efficiency and after-treatment systems. The exhaust gas temperature slightly increased, and the fuel consumption decreased by 0.5% under the WLTC. Rohil et al. [146] simulated a vacuum-insulated catalytic converter. CO and HC emissions decreased by 26% and 48%, respectively, at real-world driving conditions. Wang et al. [147] applied a layer of 6 mm insulation material to the exhaust pipe in a section between the turbine outlet and the DOC, which reduced NO_x emission by 19.5% under the NRTC. Wang et al. [148] increased the in-cylinder temperature by 100–200 K via a thermal barrier coating, which indirectly increased the exhaust gas temperature. Luján et al. [149] investigated the effects of exhaust port insulation and turbocharger insulation on exhaust temperature and fuel consumption. Four cases of exhaust port insulation strategies are shown in Figure 11b. The inlet temperature followed a trend of 4 > 3 > 2 > 1, and the BSFC followed a trend of 1 > 2 ≈ 3 > 4. The thermal insulation strategy of the turbocharger affected insignificantly the inlet temperature of the after-treatment system and BSFC. Thermal insulation methods can improve exhaust temperatures, but they do not provide additional heat. Thus, thermal insulation methods cannot be used as a final solution.

4.4. PCMs and the Heat Recovery System

PCMs release or absorb a large amount of heat during phase change to heat or cool down [150,151]. PCMs can be used to recover waste heat and improve energy utilization. PCMs have been widely implemented in automobiles [152,153]. PCMs are implemented in the after-treatment system to recover heat under high load conditions and then release energy under low load conditions to improve catalyst performance.

Korin et al. [154] embedded a 3.8 kg PCM into the TWC. After the engine turned off, the TWC remained above the light-off temperature for 4 h, which benefited from the heat release of the PCM. If the engine turns on again within 4 h, the emission under cold start conditions will be improved, but the PCM will not work if the engine starts after 4 h. Gaiser et al. [155] adopted a PCM with a phase change temperature higher than the catalytic converter light-off temperature and installed a latent heat storage (LHS) device upstream of the catalytic converter to heat the exhaust gas using the fact that the temperature of the PCM in the LHS did not change when it melted. The catalyst inlet temperature reached 200 °C within 100 s and remained around 200 °C in the following 400 s under the cold start condition. Hamed et al. [156] developed a thermal energy storage system (TES) based on a PCM to reduce cold start emissions (as shown in Figure 11c). Under the NEDC, the DOC equipped with TES reduced CO and HC emissions by 64% and 34%, respectively.

Jiang et al. [129] limited the temperature fluctuation of SCR to 30 K via PCM. Raznoshinskaia et al. [157] decreased the range of exhaust temperature vibrations by 73.1% with the ternary eutectic mixture of 7NaNO₃/40NaNO₂/53KNO₃. PCMs are a potential way to stabilize the exhaust temperature. Dae et al. [158] developed an engine exhaust heat recovery system (EERS) equipped with secondary combustion. Exhaust gas temperatures increased from 200–350 °C to 350–550 °C due to the combustor, which was installed at the outlet of the exhaust manifold (Figure 11d). The EERS improved thermal efficiency up to 20–25% and decreased CO, NO_x, and PM emissions by 80%, 35%, and 90%, respectively. Park et al. [159] adopted the heat storage system of a PCM for a 1.6 L diesel engine. The time to warm up the coolant to 95 °C was reduced by 40.5% under the NEDC, and fuel consumption was reduced by 2.71%. Gumus et al. [160] utilized PCMs to preheat the engine, which improved emissions during cold start. The HC and CO emissions decreased by 17.32% and 28.71%, respectively.

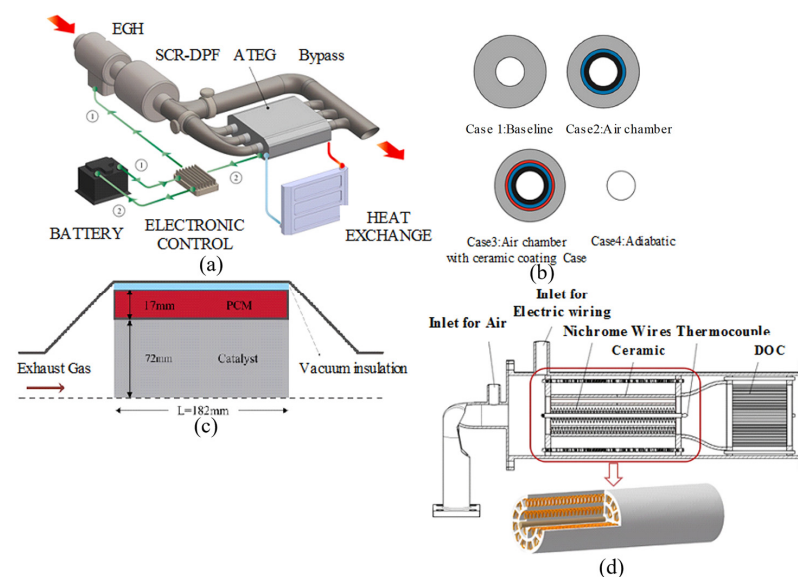


Figure 11. Structures of exhaust gas after-treatment devices and components in various studies. (a) Structure and energy flow of EGH-ATEG [144]. ① heating stage; ② recovery stage. (b) Representation of exhaust ports thermal insulation cases [149]. (c) PCM model geometry diagram [156]. (d) Schematic diagram of secondary combustor [158].

Table 2 is a summary of the reduction in exhaust emissions by the above after-treatment thermal management technologies.

Table 2. Performance improvement of exhaust after-treatment systems by different technologies.

Technologies	Test Conditions	Effect on Pollutants in Exhaust Gas				
		HC	CO	PM	NO _x	CO ₂
Burner [131]	LLC	N.A.	N.A.	N.A.	↓93.5%	↑9%
EHC [138]	Cold WLTC	↓80%	↓80%	N.A.	↓66%	↑9.35%
EHC + CDA [142]	Cold FTP compared with CDA	N.A.	N.A.	N.A.	↓12.5%	↓0.7%
Insulation methods [146]	Real-world driving	↓48%	↓26%	N.A.	N.A.	N.A.
PCM-based TES [156]	NEDC	↓41.2%	↓91.7%	N.A.	N.A.	N.A.
EERS [158]	Water flow of 20 L/min and a power generation of 9 kW	N.A.	↓80%	↓90%	↓35%	N.A.

4.5. VVT and Post Injection

Arnau et al. [161] investigated the effects of VVT on exhaust temperature, DOC light-off time, and fuel consumption. The combination of an advanced exhaust and a delayed intake obtained a 27 °C increase in DOC inlet temperature, 75 s reduction in DOC light-off time, and 6% deterioration in fuel consumption during the low-speed phase of the worldwide harmonized light vehicles test cycle. Wu et al. [85] combined thermal insulation, post injection, and VGT-RIVCT under cold WHTC to enable the SCR to reach 190 °C at 450 s, which could significantly reduce NO_x emission. CDA is achieved by adjusting valve movement and stopping in-cylinder fuel injection. CDA is a technology to reduce fuel consumption [162,163]. The benefit is achieved in part-load operations when the BSFC is higher than in full-load operations [164]. CDA is also an effective method to increase the exhaust temperature [165,166]. Ramesh et al. [167] increased exhaust temperature by 60 °C and improved BTE up to 10% with a three-cylinder strategy at a condition of 800 rpm and 1.3 bar BMEP. A two-cylinder strategy increased the exhaust temperature by 120 °C and improved BTE up to 2%. Allen et al. [168] explored the performance of CDA to maintain warmth for the after-treatment system at an extended idle operation. The result showed that the turbine outlet temperature was maintained above 250 °C with a two-cylinder strategy.

Internal exhaust gas recirculation (IEGR) is achieved with both negative valve overlap (NVO) and reinduction [169]. Joshi et al. [170] confirmed that EEVO/NVO increased the exhaust temperature to more than 255 °C and decreased fuel consumption by 5.7%. Simultaneously, LEVO took the exhaust temperature to above 280 °C with no extra fuel consumption. Wang et al. [171] explored the effects of post injection timing on engine-out HC emission, exhaust temperature, and torque, as displayed in Figure 12a,b.

With the delay in the post injection timing, the exhaust temperature increased and then decreased. The later the post injection timing was, the less fuel participated in the combustion, which resulted in a deterioration in torque. The fuel consumption and the HC entering the exhaust pipe increased (Figure 12c), which intensified the reaction of the DOC and raised the DOC outlet temperature.

Huang et al. [172] developed a DPF temperature control strategy based on post injection. The control strategy calculated the quantity of post injection based on the target regeneration temperature and amended the quantity via feedback and feedforward compensation methods based on both the exhaust gas temperature and flow rate. As shown in Figure 13a,b, after the DPF inlet temperature reached the target regeneration temperature, its fluctuation was within 15 °C under different urban driving conditions, which proved the robustness of the control strategy.

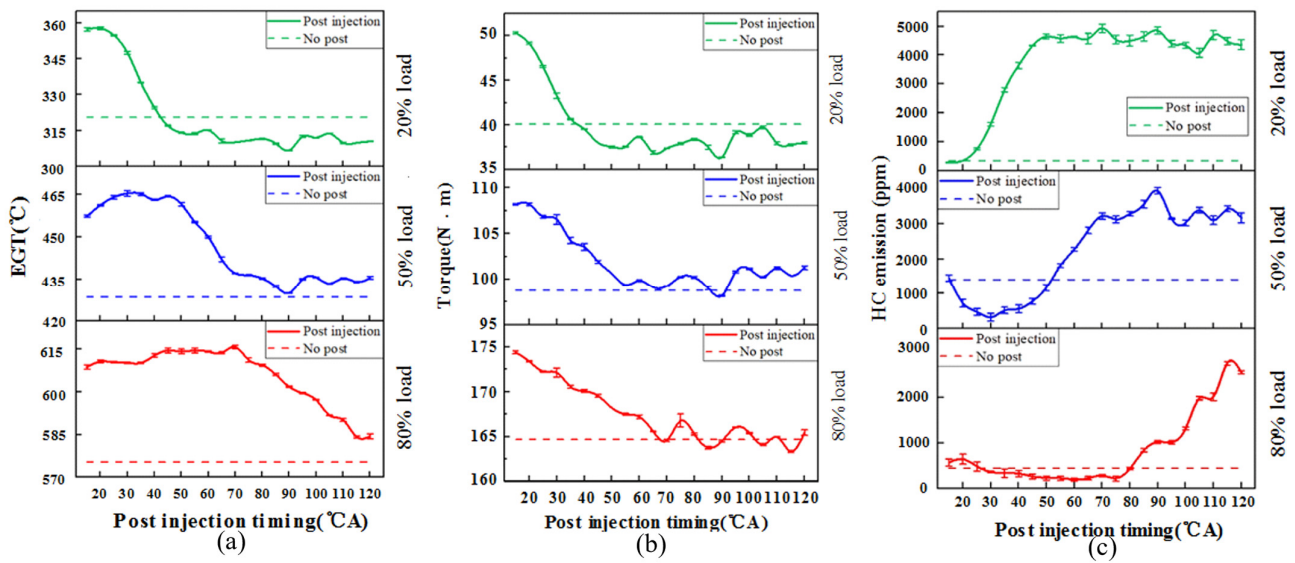


Figure 12. Effects of post injection on torque and HC [171]. (a) Effects of post injection on EGT at different loads. (b) Effects of post injection on engine brake torque at different loads. (c) Effects of post injection on HC at different loads.

4.6. Catalysts

Catalysts with high activity and thermal stability improved the efficiency of the after-treatment system and reduced the energy consumption of the thermal management. Pt-based catalysts are the most widely used catalysts in DOCs [173,174]. Kolli et al. [175] and Boubnov et al. [176] confirmed that Pt/Al₂O₃ had a high catalytic activity and a poor sulfur resistance. As shown in Figure 14a', Liang et al. [177] loaded Pt on MnO_x, which enhanced the catalytic activity of Pt. The conversions of CO, C₃H₆, and NO_x are given in Figure 14b'–d'. Väliheikki et al. [178] and Gu et al. [179] adopted SiO₂-ZrO₂ and Ce-Zr-SO₄²⁻ as supports to improve the sulfur resistance and stability of Pt-based catalysts.

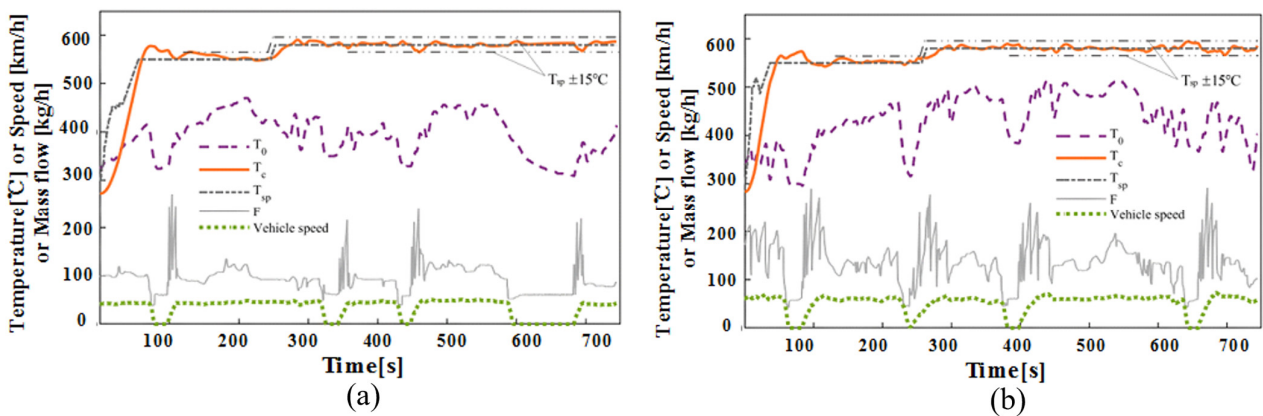


Figure 13. Test results of different conditions [172]. (a) Test results under urban driving conditions. (b) Test results under aggressive suburban driving conditions.

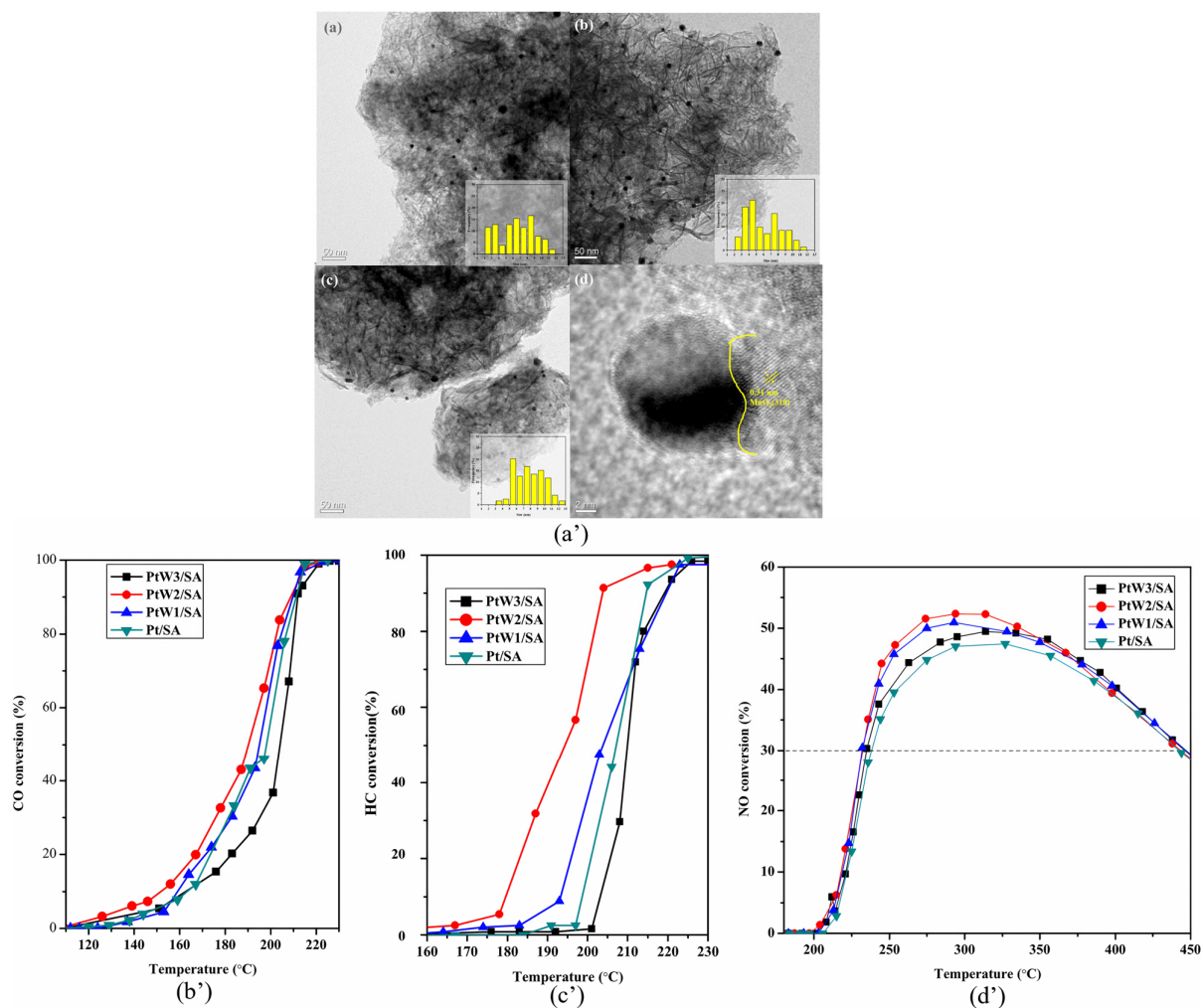


Figure 14. Conversion of all catalysts (Rx, “x” represents the reaction temperature of manganese oxide reduction) [177]. (a’) TEM images of catalyst: (a) R200, (b) R250, (c) 300, and the corresponding particle size distribution is inserted as a histogram; (d) HRTEM image of R250. (b’) CO conversion of all catalysts. (c’) C₃H₆ conversion of all catalysts. (d’) NO conversion of all catalysts.

The researchers reported that doping with other metals can enhance the performance of Pt-based catalysts. Liang et al. [180] added 2%wt tungsten trioxide (WO₃) to Pt/SiO₂-Al₂O₃, and the light-off temperature of HC and CO was reduced. Kim et al. [181] reported the relationship between the value of Pd/Pt and light-off temperature and the relationship between thermal stability and the value of Pd/Pt (Figure 15a). E et al. [16] indicated that the light-off temperature of the Pt-Pd catalyst was lowest when the Pd was approximately 70%. Huang et al. [182] doped the Pt/Ce-Zr-O catalyst with vanadium (V) (Figure 15b). The CO and HC light-off temperatures of 1Pt-1V/Ce-Zr-O were approximately 195 °C and 190 °C, respectively. Furthermore, the light-off temperature of HC was almost constant, and the light-off temperature of CO increased by 10 °C in an SO₂ atmosphere for 70 h.

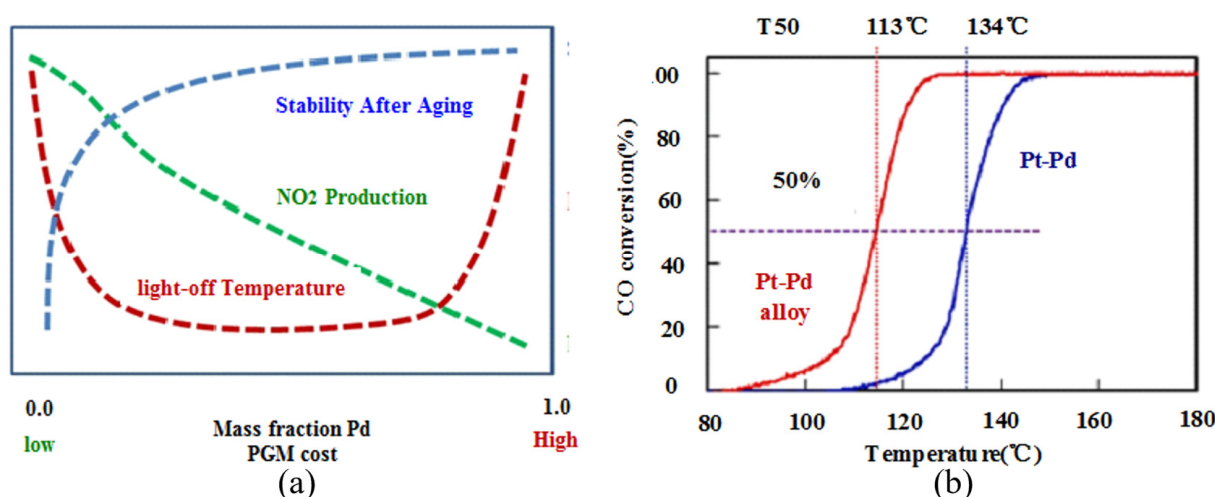


Figure 15. Catalytic activity or stability of each series of catalysts. (a) Pt to Pd ratio effect on Pt-based diesel oxidation catalysts [181]. (b) Catalytic activities of CO on the Pt-Pd alloy catalyst and the conventional Pt-Pd catalyst [16].

The researchers developed alloy catalysts that were better than conventional catalysts. Dong et al. [183] investigated a Pt (1.0 wt%)-Pd (0.5 wt%) alloy catalyst loaded on SiO₂. The activity of the Pt-Pd alloy catalyst was higher than the conventional Pt-Pd catalyst. Franken et al. [184] confirmed that the Mn-Pt alloy catalyst is a sulfur-tolerant catalyst. The conversion of NO_x deteriorated by 6% under the 300 ppm SO₂ for 70 h, while the pure Pt/Al₂O₃ catalyst deactivated fully within the first 30 min. Ceria (CeO₂) catalysts, which are rare-earth metal catalysts, are widely applied in automotive exhaust after-treatment systems [185,186]. Bueno-López et al. [187] reported that the temperature at which CeO₂ reached 50% soot conversion rate was 525 °C. Ce-based catalysts can be doped with rare-earth metals [188,189], noble metals [190,191], transition metals [192,193], alkali metals [194,195], and alkaline earth metals [196]. Yang et al. [197] added Mn to improve the activity of soot oxidation and the thermal stability of Ce-based catalysts. The T₁₀ of the 40% Mn-Ce catalyst was 475 °C, and the T₉₀ was 565 °C. Stability of the 40% Mn-Ce catalyst decreased in the third cycle of the thermo-gravimetric analyzer experiment. Atribak et al. [198] revealed that doping zirconium (Zr) improved the thermal stability of Ce-based catalysts. Yang et al. [199] added lanthanum (La) to the CeO₂-ZrO₂ catalyst and tested the catalytic activity of soluble organics (SOs). The test result indicated that the catalyst was more active and had a slower aging rate after doping with La. Wu et al. [200] studied the catalytic activity of CeZrK/rGO with different doping ratios. The T₅₀ of Ce₅Zr₁K₁/rGO, Ce₅Zr₂K₂/rGO, and Ce₅Zr₃K₃/rGO for soot oxidation were 352 °C, 339 °C, and 358 °C, respectively (Figure 16).

Sarli et al. [201] added Ag to CeO₂, which greatly enhanced the catalytic activity. The T₁₀ of 12% Ag/CeO₂ for soot oxidation was 240 °C, and the temperature at maximum conversion was 435 °C. At present, various transition metal catalysts have been investigated. Cheng et al. [202] investigated a series of V₂O₅/TiO₂ catalysts to improve the catalytic performance of NH₃-SCR. The results showed that the NO conversion efficiency was above 80% when the 5% V₂O₅/TiO₂ supported on aluminate was at temperatures between 325 °C and 400 °C. Ding et al. [203] prepared the MFe₂O₄ (M = Cu, Mn, and Zr) (Figure 17a). As shown in Figure 17b,c, MnFe₂O₄ had the highest activity, and ZnFe₂O₄ had the highest N₂ selectivity, at low temperatures. CuFe₂O₄ was a balanced catalyst, but its efficient reaction temperature range is narrow. In addition, the catalytic activity of CuFe₂O₄ decreased by 8% in SO₂ atmosphere for about 2 h. Zhang et al. [204] reviewed Mn-based catalysts for NH₃-SCR and summarized the advantages and disadvantages of MnO_x. MnO_x had a high low-temperature activity and played a decisive role in the SCR reaction but had poor thermal stability and a narrow reaction temperature window. It also had an insufficient reaction in the eutrophic environment and weak sulfur resistance.

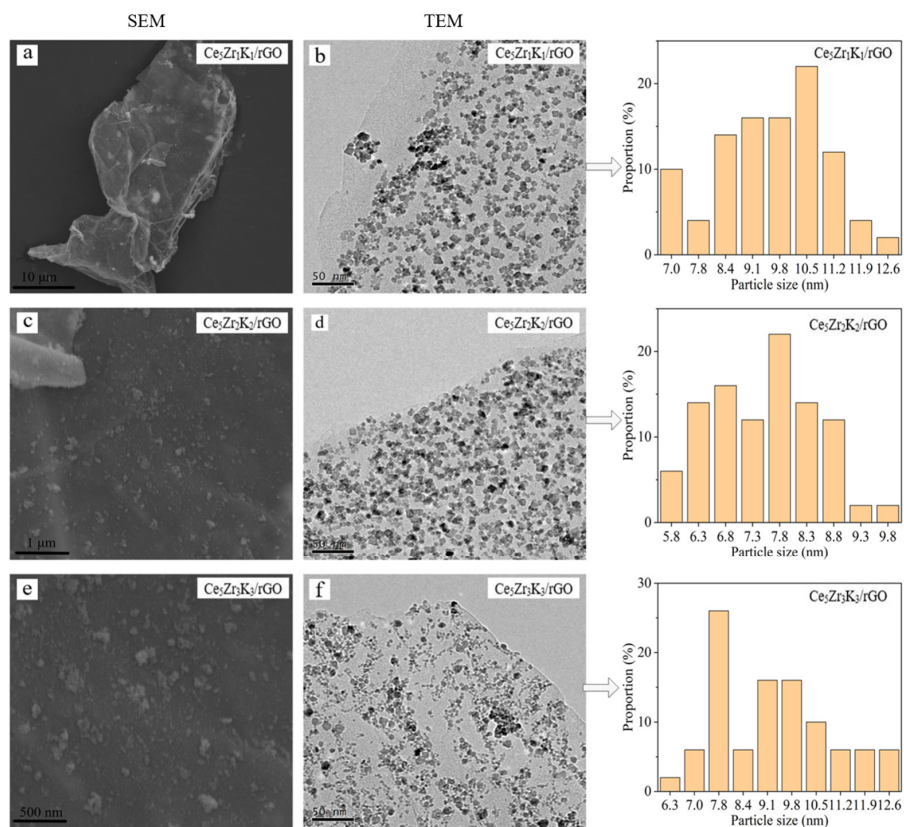


Figure 16. SEM and TEM images of CeZrK/rGO catalysts ((a,c,e) are SEM images. (b,d,f) are TEM images.) [200].

To reduce the cost and enhance the activity and stability of the catalysts, Tang et al. [205] developed a LaKCoO₃/γ-Al₂O₃/cordierite perovskite catalyst. The results showed the high activity and thermal stability of the LaKCoO₃/γ-Al₂O₃/cordierite. The T₁₀, T₅₀, and T₉₀ of the LaKCoO₃/γ-Al₂O₃/cordierite catalyst for soot oxidation were 186.3 °C, 314.6 °C, and 390.0 °C, respectively.

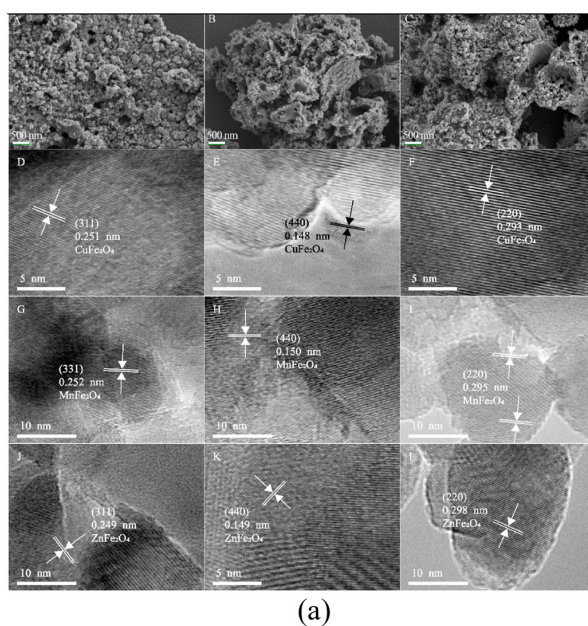


Figure 17. Cont.

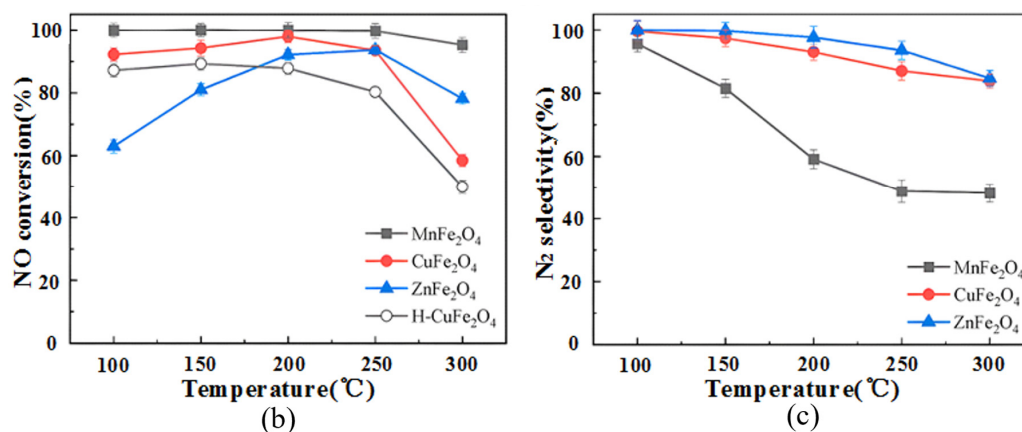


Figure 17. Data of MFe_2O_4 ($M = Cu, Mn, \text{ and } Zn$) [200]. (a) SEM of $CuFe_2O_4$ (A), $MnFe_2O_4$ (B), and $ZnFe_2O_4$ (C); HRTEM of $CuFe_2O_4$ (D–F), $MnFe_2O_4$ (G–I), and $ZnFe_2O_4$ (J–L) [203]. (b) NO_g conversion vs. temperature ($GHSV = 30,000 \text{ h}^{-1}$). (c) N_2 selectivity vs. temperature ($GHSV = 30,000 \text{ h}^{-1}$).

5. Outlook for Future Research

5.1. Shortcomings of Current Technologies

The engine-based after-treatment management methods increase the exhaust temperature, and the high-temperature flowing exhaust gas heats the after-treatment devices, which can shorten the light-off time of the after-treatment system. These methods do not require additional devices and are relatively simple to implement. However, changing the engine parameters leads to fuel economy penalties. Techniques such as intake and exhaust throttling [85] or EVO timing technology [82] lead to worse combustion and a deterioration in BTE. CDA and IVC timing can increase exhaust temperature and improve fuel consumption [161,167]. The low-flow-rate strategies reduce the exhaust flow rate, and the exhaust gas has a longer contact time with the exhaust pipe, which leads to more heat dissipation to the atmosphere [83,168]. Fuel strategies such as post injection and hydrocarbon injection directly convert the chemical energy of fuel to thermal energy to increase the temperature of the after-treatment system [171,172]. Energy conversion efficiency is a problem that needs to be considered, and these fuel strategies lead to higher fuel consumption [85,171]. Post injection can also lead to oil dilution, affecting the life of the engine [102].

Technologies such as burners, EHCs, and microwave heating have proven to be effective thermal management measures that are flexible and easy to control, but the control strategy cannot coordinate the entire after-treatment system [131,138]. For example, when the burner and EHC are installed upstream of the after-treatment system, the heat produced has a relatively weak effect on the SCR downstream of the after-treatment system. The conversion rate of NO_x is lower compared with HC and CO [131,138]. The DPF outlet temperature can be considered the SCR threshold temperature while ignoring the DOC [131,133].

The heat recovery system based on the PCM for the after-treatment system thermal management can solve the trade-off problem of exhaust gas temperature and carbon dioxide emission, but the PCMs are effective only when the engine is turned on again before the PCM heat is exhausted [156]. PCMs are a potential method to stabilize exhaust temperatures [157]. The thermoelectric generator recovers a part of the electric energy through the exhaust heat and compensates for the EHC. The thermoelectric generator increases the complexity of the after-treatment system, which can increase the back pressure [143,144].

Simulation research under adiabatic conditions has confirmed that the thermal insulation methods are able to shorten the light-off time of the after-treatment system, but the currently developed thermal insulation methods still have a certain gap in the adiabatic case. The developed catalysts have high activity at low temperatures [174,183]. The reaction temperature window is narrow for SCR [203,204]. The anti-deterioration performance is still a challenge (anti-sulfur, phosphorus, etc.) [49,204].

5.2. Outlook for Future Technologies

As described in the previous section, there are limitations in the separate technical methods, and multiple technologies need to be combined to improve the efficiency of after-treatment thermal management technology. Future technologies can be further explored from the following aspects:

- (1) To optimize CO₂ emissions and exhaust temperatures, control strategies for the EHC and post injection coupled methods are investigated [137].
- (2) The active and passive thermal management technologies are combined [85,156].
- (3) Further control strategies for EHC [138,139], burners [132,133], and late post injection [168], based on the entire after-treatment system, are applied.
- (4) Materials are used with lower thermal conductivity and different insulation methods to approach adiabatic conditions [145,149] for better PCM development [156,157].
- (5) The inexpensive catalysts' improvement is developed widely to explore catalysts with excellent degradation resistance [204,205].

6. Conclusions

Although combustion technology [206,207] and alternative fuels [208,209] are constantly improving, increasingly stringent emission regulations promote the development of advanced technologies in the after-treatment systems of internal combustion engines [210,211]. After-treatment systems still have the shortcoming that they require strict temperature conditions to efficiently convert pollutants [212,213]. At too low or too high a temperature, the after-treatment devices are at a low conversion efficiency level [214,215]. This thermal heat can be converted into electrical energy, as shown in the latest research [216,217]. The investigation of diesel after-treatment thermal management is summarized. After-treatment thermal management can improve the efficiency of after-treatment devices and reduce emissions, but the trade-off problem between thermal efficiency and exhaust gas temperature is still a challenge. The technical advantages and application potential of after-treatment thermal management are valuable to carry out in-depth research. The main conclusions of this study are as follows.

- (1) SCR burners can decrease NO_x emissions by 93.5%. EHC can decrease CO, HC, and NO_x emissions by 80%, 80%, and 66%, respectively. PCMs can control the temperature of SCR, resulting in a 2/3 reduction in NO_x emissions.
- (2) Thermal insulation decreases the heat loss of the exhaust gas, which can reduce the after-treatment light-off time. DOC light-off time was reduced by 75% under adiabatic conditions. Microwave is an effective method for DPF regeneration. A 400 W microwave can heat the DPF to the soot oxidation temperature of 873 K at a regeneration time of 150 s.
- (3) Catalysts can enhance the efficiency of the after-treatment system and reduce the thermal management energy consumption. Pt-Pd application in the catalyst can decrease the CO light-off temperature to 113 °C. The LaKCoO₃/γ-Al₂O₃/cordierite catalyst with a T₅₀ of 314.6 °C for soot oxidation can reduce the regeneration target temperature.
- (4) The future research trends focus on integration of engine-based and non-engine-based thermal management methods, control strategies of EHCs, insulation methods with low thermal conductivity, catalysts with excellent degradation resistance, and the implementation of these thermal management methods under transient operating conditions.

Funding: This work is supported by the National Natural Science Foundation of China (Grant No. 51976016), the Young Scientists Fund of the National Natural Science Foundation of China (Grant No. 52106151), and the Natural Science Foundation of Hunan Province, China (Grant No. 2020JJ4616).

Conflicts of Interest: Authors Tao Ling, Xuejun Peng, Zhilai Su were employed by the company China Railway Wuju Group First Engineering Co., Ltd. The remaining authors declare that the research was conducted in the absence of any commercial or financial relationships that could be construed as a potential conflict of interest.

Nomenclature

Compounds

Al ₂ O ₃	Alumina
CO	Carbon monoxide
CO ₂	Carbon dioxide
CeO ₂	Cerium dioxide
HC	Hydrocarbon
H ₂ O	Water
MnO _x	Manganese oxides
N ₂	Nitrogen
NO _x	Nitrogen oxides
NO ₂	Nitrogen dioxide
NO	Nitric oxide
N ₂ O	Nitrous oxide
NH ₂ CONH ₂	Urea
NH ₃	Ammonia gas
O ₂	Oxygen
PM	Particulate matter
SOs	Soluble organics
SO ₄ ²⁻	Sulfate
SiO ₂	Silicon dioxide
TiO ₂	Titanium oxide
V ₂ O ₅	Vanadium oxide
WO ₃	Tungsten oxide
ZrO ₂	Zirconium dioxide

Abbreviations

ASC	Ammonia slip catalyst
ATDC	After top dead center
ATEG	Automotive thermoelectric generator
BMEP	Brake mean effective pressure
BSFC	Brake-specific fuel consumption
BTDC	Before top dead center

BTE	Brake thermal efficiency
CA	Crank angle
CDA	Cylinder deactivation
CFD	Computational fluid dynamics
CDPF	Catalytic diesel particulate filter
DOC	Diesel oxidation catalyst
DPF	Diesel particulate filter
DTI	Drop to idle
EEHRS	Engine exhaust heat recovery system
EEVO	Early exhaust valve opening
EGR	Exhaust gas recirculation
EGT	Exhaust gas temperature
EHC	Electrically heated catalyst
EH	Electric heating
EIVC	Early intake valve closing
EM	Exhaust manifold
EP	Exhaust port
ETC	European transient cycling
EVO	Exhaust valve opening
FTP	Federal test procedure
FTP75	Environmental Protection Agency Federal Test Procedure
IEGR	Internal exhaust gas recirculation
IVC	Intake valve closing
LEVO	Late exhaust valve opening
LHS	Latent heat storage
LIVC	Late intake valve closing
LLC	Low load cycle
NEDC	New European driving cycle
NRTC	Non-road transient cycle
NVO	Negative valve overlap
PCM	Phase-change material
RIVCT	Retarded intake valve closing timing technology
RDPF	Rotary diesel particulate filter
SCR	Selective catalytic reduction
SEM	Scanning electron microscopy
TEM	Transmission electron microscopy
TESS	Thermal energy storage system
TI	Internal surface of the turbine volute
TWC	Three-way catalyst
VGT	Variable geometry turbine
VVT	Variable valve timing
WHTC	World harmonized transient cycle
WLTC	World light vehicle test cycle
Symbols	
c_p	Specific heat of the exhaust gas, kJ/kg/K
H	Lower heating value of the diesel fuel, kJ/kg
\dot{m}_{exhaust}	Mass flow rate of the exhaust gas, kg/h
R_{TU}	Temperature uniformity coefficient
$\Delta T_{\text{exhaust}}$	Difference between target exhaust temperature and incoming exhaust temperature, K
T_j	Temperature of a position in the wall-flow filter, K
\bar{T}	The wall-flow filter's average temperature under a certain condition, K

References

1. Jiaqiang, E.; Zuo, W.; Gao, J.; Peng, Q.; Zhang, Z.; Hieu, P.M. Effect analysis on pressure drop of the continuous regeneration-diesel particulate filter based on NO₂ assisted regeneration. *Appl. Therm. Eng.* **2016**, *100*, 356–366.
2. Jiaqiang, E.; Zhao, X.; Qiu, L.; Wei, K.; Zhang, Z.; Deng, Y.; Han, D.; Liu, G. Experimental investigation on performance and economy characteristics of a diesel engine with variable nozzle turbocharger and its application in urban bus. *Energy Convers. Manag.* **2019**, *193*, 149–161.

3. Serrano, J.R. Imagining the future of the internal combustion engine for ground transport in the current context. *Appl. Sci.* **2017**, *7*, 1001. [[CrossRef](#)]
4. Backhaus, R. We still need diesel engines. *MTZ Worldw.* **2019**, *80*, 6–7. [[CrossRef](#)]
5. Reşitoğlu, İ.A.; Altinişik, K.; Keskin, A. The pollutant emissions from diesel-engine vehicles and exhaust after-treatment systems. *Clean Technol. Environ. Policy* **2015**, *17*, 15–27. [[CrossRef](#)]
6. Di Natale, F.; Carotenuto, C. Particulate matter in marine diesel engines exhausts: Emissions and control strategies. *Transp. Res. Part D Transp. Environ.* **2015**, *40*, 166–191. [[CrossRef](#)]
7. Kim, Y.S.; Han, E.J.; Sohn, S.Y. Demand forecasting for heavy-duty diesel engines considering emission regulations. *Sustainability* **2017**, *9*, 166. [[CrossRef](#)]
8. Rubio, F.; Llopis-Albert, C.; Valero, F.; Besa, A.J. Sustainability and optimization in the automotive sector for adaptation to government vehicle pollutant emission regulations. *J. Bus. Res.* **2020**, *112*, 561–566. [[CrossRef](#)]
9. Russell, A.; Epling, W.S. Diesel oxidation catalysts. *Catal. Rev.-Sci. Eng.* **2011**, *53*, 337–423. [[CrossRef](#)]
10. Zhang, Z.; Cheung, C.; Chan, T.; Yao, C. Emission reduction from diesel engine using fumigation methanol and diesel oxidation catalyst. *Sci. Total Environ.* **2009**, *407*, 4497–4505. [[CrossRef](#)]
11. Yang, S.; Deng, C.; Gao, Y.; He, Y. Diesel particulate filter design simulation: A review. *Adv. Mech. Eng.* **2016**, *8*, 1–14. [[CrossRef](#)]
12. Li, J.; Ge, Y.; Wang, H.; Yu, C.; Yan, X.; Hao, L.; Tan, J. Effects of different diesel particulate filter on emission characteristics of in-use diesel vehicles. *Energy Sources Part A-Recovery Util. Environ. Eff.* **2019**, *41*, 2989–3000. [[CrossRef](#)]
13. Wang, J.; Zhao, H.; Haller, G.; Li, Y. Recent advances in the selective catalytic reduction of NO_x with NH₃ on Cu-Chabazite catalysts. *Appl. Catal. B Environ.* **2017**, *202*, 346–354. [[CrossRef](#)]
14. Zhang, R.; Quan, X.; Yang, F.; Chung, J.S. Selective catalytic reduction of NO with NH₃ on wire mesh honeycomb. *Chin. J. Catal.* **2002**, *23*, 46–50.
15. Gao, J.; Tian, G.; Sornioti, A.; Karci, A.E.; Di Palo, R. Review of thermal management of catalytic converters to decrease engine emissions during cold start and warm up. *Appl. Therm. Eng.* **2019**, *147*, 177–187. [[CrossRef](#)]
16. E, J.; Luo, J.; Han, D.; Tan, Y.; Feng, C.; Deng, Y. Effects of different catalysts on light-off temperature of volatile organic components in the rotary diesel particulate filter during the regeneration. *Fuel* **2022**, *310*, 122451.
17. Zare, A.; Nabi, M.N.; Bodisco, T.A.; Hossain, F.M.; Rahman, M.M.; Van, T.C.; Ristovski, Z.D.; Brown, R.J. Diesel engine emissions with oxygenated fuels: A comparative study into cold-start and hot-start operation. *J. Clean. Prod.* **2017**, *162*, 997–1008. [[CrossRef](#)]
18. Chaichan, M.T.; Maroon, O.K.; Abaas, K.I. The effect of diesel engine cold start period on the emitted emissions. *Int. J. Sci. Eng. Res.* **2016**, *7*, 749–753.
19. Deng, Y.; Liu, H.; Zhao, X.; Jiaqiang, E.; Chen, J. Effects of cold start control strategy on cold start performance of the diesel engine based on a comprehensive preheat diesel engine model. *Appl. Energy* **2018**, *210*, 279–287. [[CrossRef](#)]
20. Robinson, K.; Ye, S.; Yap, Y.; Kolaczowski, S.T. Application of a methodology to assess the performance of a full-scale diesel oxidation catalyst during cold and hot start NEDC drive cycles. *Chem. Eng. Res. Des.* **2013**, *91*, 1292–1306. [[CrossRef](#)]
21. Maus, W.; Brück, R.; Konieczny, R.; Scheeder, A. Electrically heated catalyst for thermal management in modern vehicle applications. *MTZ Worldw.* **2010**, *71*, 34–39. [[CrossRef](#)]
22. Mera, Z.; Fonseca, N.; Casanova, J.; López, J.M. Influence of exhaust gas temperature and air-fuel ratio on NO_x after-treatment performance of five large passenger cars. *Atmos. Environ.* **2021**, *244*, 117878. [[CrossRef](#)]
23. Birkhold, F.; Meingast, U.; Wassermann, P.; Deutschmann, O. Modeling and simulation of the injection of urea-water-solution for automotive SCR DeNO_x-systems. *Appl. Catal. B Environ.* **2007**, *70*, 119–127. [[CrossRef](#)]
24. Kim, H.J.; Jo, S.; Kwon, S.; Lee, J.T.; Park, S. NO_x emission analysis according to after-treatment devices (SCR, LNT + SCR, SDPF), and control strategies in Euro-6 light-duty diesel vehicles. *Fuel* **2022**, *310*, 122297. [[CrossRef](#)]
25. Prasad, R.; Singh, S.V. A review on catalytic oxidation of soot emitted from diesel fuelled engines. *J. Environ. Chem. Eng.* **2020**, *8*, 103945.
26. Orihuela, M.P.; Chacartegui, R.; Gómez-Martín, A.; Ramírez-Rico, J.; Villanueva, J.A.B. Performance trends in wall-flow diesel particulate filters: Comparative analysis of their filtration efficiency and pressure drop. *J. Clean. Prod.* **2020**, *260*, 120863. [[CrossRef](#)]
27. Han, L.; Cai, S.; Gao, M.; Hasegawa, J.Y.; Wang, P.; Zhang, J.; Shi, L.; Zhang, D. Selective catalytic reduction of NO_x with NH₃ by using novel catalysts: State of the art and future prospects. *Chem. Rev.* **2019**, *119*, 10916–10976. [[CrossRef](#)]
28. Zhong, F.; Zhong, Y.; Xiao, Y.; Cai, G.; Wei, K. Effect of Si-doping on thermal stability and diesel oxidation activity of Pt supported porous γ -Al₂O₃ monolithic catalyst. *Catal. Lett.* **2011**, *141*, 1828–1837. [[CrossRef](#)]
29. Bai, S.; Han, J.; Liu, M.; Qin, S.; Wang, G.; Li, G. Experimental investigation of exhaust thermal management on NO_x emissions of heavy-duty diesel engine under the world Harmonized transient cycle (WHTC). *Appl. Therm. Eng.* **2018**, *142*, 421–432. [[CrossRef](#)]
30. Honardar, S.; Busch, H.; Schnorbus, T.; Severin, C.; Kolbeck, A.F.; Korfer, T. Exhaust temperature management for diesel engines assessment of engine concepts and calibration strategies with regard to fuel penalty. In Proceedings of the 10th International Conference on Engines & Vehicles, Naples, Italy, 10–14 September 2023.
31. Brin, J.W.; Keim, J.A.; Christensen, E.T.; Holman, R.S. Applying a driven turbocharger with turbine bypass to improve after-treatment warm-up and diesel nitrous oxides conversion. *SAE Int. J. Commer. Veh.* **2021**, *14*, 391–407. [[CrossRef](#)]
32. Salehi, R.; Stefanopoulou, A.G. Optimal exhaust valve opening control for fast after-treatment warm up in diesel engines. In Proceedings of the ASME 2018 Dynamic Systems and Control Conference, Atlanta, GA, USA, 30 September–3 October 2018.

33. Kovacs, D.; Rauch, H.; Rezaei, R.; Huang, Y.; Harris, T. Modeling heavy-duty engine thermal management technologies to meet future cold start requirements. In Proceedings of the WCX SAE World Congress Experience, Detroit, MI, USA, 9–11 April 2019.
34. Hamedi, M.; Tsolakis, A.; Herreros, J.M. Thermal Performance of Diesel After-treatment: Material and Insulation CFD Analysis. In Proceedings of the SAE 2014 International Powertrain, Fuels & Lubricants Meeting, Birmingham, UK, 20–22 October 2014.
35. Burch, S.D.; Potter, T.F.; Keyser, M.A.; Brady, M.J.; Michaels, K.F. Reducing cold-start emissions by catalytic converter thermal management. In *SAE Transactions*; National Renewable Energy Laboratory: Golden, CO, USA, 1995; pp. 348–353.
36. Feng, X.; Ge, Y.; Tan, J.; Li, J.; Zhang, Y.; Yu, C. Effects of electrically heated catalyst on the low temperature performance of vanadium-based SCR catalyst on diesel engine. In Proceedings of the SAE 2014 World Congress & Exhibition, Detroit, MI, USA, 8–10 April 2014.
37. Miao, Y.; Chen, L.-D.; He, Y.; Kuo, T.-W. Study of SCR cold-start by energy method. *Chem. Eng. J.* **2009**, *155*, 260–265. [[CrossRef](#)]
38. Ma, T.; Collings, N.; Hands, T. Exhaust gas ignition (EGI)-a new concept for rapid light-off of automotive exhaust catalyst. *SAE Trans.* **1992**, *101*, 595–599.
39. Sharp, C.; Webb, C.C.; Neely, G.; Carter, M.; Yoon, S.; Henry, C. Achieving ultra-low NO_x emissions levels with a 2017 heavy-duty on-highway TC diesel engine and an advanced technology emissions system-thermal management strategies. *SAE Int. J. Engines* **2017**, *10*, 1697–1712. [[CrossRef](#)]
40. Kurien, C.; Srivastava, A.K.; Lesbats, S. Experimental and computational study on the microwave energy-based regeneration in diesel particulate filter for exhaust emission control. *J. Energy Inst.* **2020**, *93*, 2133–2147. [[CrossRef](#)]
41. Yang, W.; Gong, J.; Wang, X.; Bao, Z.; Guo, Y.; Wu, Z. A Review on the Impact of SO₂ on the Oxidation of NO, Hydrocarbons, and CO in Diesel Emission Control Catalysis. *ACS Catal.* **2021**, *11*, 12446–12468. [[CrossRef](#)]
42. Hoang, S.; Lu, X.; Tang, W.; Wang, S.; Du, S.; Nam, C.-Y.; Ding, Y.; Vinluan, R.D.; Zheng, J.; Gao, P.-X. High performance diesel oxidation catalysts using ultra-low Pt loading on titania nanowire array integrated cordierite honeycombs. *Catal. Today* **2019**, *320*, 2–10. [[CrossRef](#)]
43. Nadanakumar, V.; Muthiya, S.J.; Prudhvi, T.; Induja, S.; Sathyamurthy, R.; Dharmaraj, V. Experimental investigation to control HC, CO & NO_x emissions from diesel engines using diesel oxidation catalyst. *Mater. Today Proc.* **2021**, *43*, 434–440.
44. Zervas, E. Impact of different configurations of a diesel oxidation catalyst on the CO and HC tail-pipe emissions of a Euro4 passenger car. *Appl. Therm. Eng.* **2008**, *28*, 962–966. [[CrossRef](#)]
45. Gimenez-Manogil, J.; Bueno-Lopez, A.; Garcia-Garcia, A. Preparation, characterisation and testing of CuO/Ce_{0.8}Zr_{0.2}O₂ catalysts for NO oxidation to NO₂ and mild temperature diesel soot combustion. *Appl. Catal. B Environ.* **2014**, *152*, 99–107. [[CrossRef](#)]
46. Li, Z.; Zhang, W.; Chen, Z.; Jiang, Q. Mechanism of accelerating soot oxidation by NO₂ from diesel engine exhaust. *Environ. Pollut.* **2020**, *264*, 114708. [[CrossRef](#)] [[PubMed](#)]
47. Wang, W.; Herreros, J.M.; Tsolakis, A.; York, A.P. Increased NO₂ concentration in the diesel engine exhaust for improved Ag/Al₂O₃ catalyst NH₃-SCR activity. *Chem. Eng. J.* **2015**, *270*, 582–589. [[CrossRef](#)]
48. Tang, T.; Cao, D.; Zhang, J.; Zhao, Y.-G.; Shuai, S.-J. Experimental study of catalyzed diesel particulate filter with exhaust fuel injection system for heavy-duty diesel engines. In Proceedings of the SAE 2014 World Congress & Exhibition, Detroit, MI, USA, 8–10 April 2014.
49. Zhang, Z.; Tian, J.; Li, J.; Cao, C.; Wang, S.; Lv, J.; Zheng, W.; Tan, D. The development of diesel oxidation catalysts and the effect of sulfur dioxide on catalysts of metal-based diesel oxidation catalysts: A review. *Fuel Process. Technol.* **2022**, *233*, 107317. [[CrossRef](#)]
50. Lao, C.T.; Akroyd, J.; Eaves, N.; Smith, A.; Morgan, N.; Nurkowski, D.; Bhave, A.; Kraft, M. Investigation of the impact of the configuration of exhaust after-treatment system for diesel engines. *Appl. Energy* **2020**, *267*, 114844. [[CrossRef](#)]
51. Salomons, S.; Votsmeier, M.; Hayes, R.; Drochner, A.; Vogel, H.; Gieshof, J. CO and H₂ oxidation on a platinum monolith diesel oxidation catalyst. *Catal. Today* **2006**, *117*, 491–497. [[CrossRef](#)]
52. Stadlbauer, S.; Waschl, H.; Schilling, A.; del Re, L. DOC temperature control for low temperature operating ranges with post and main injection actuation. In Proceedings of the SAE 2013 World Congress & Exhibition, Detroit, MI, USA, 16–18 April 2013.
53. Guan, B.; Zhan, R.; Lin, H.; Huang, Z. Review of the state-of-the-art of exhaust particulate filter technology in internal combustion engines. *J. Environ. Manag.* **2015**, *154*, 225–258. [[CrossRef](#)]
54. Deng, Y.; Zheng, W.; Jiaqiang, E.; Zhang, B.; Zhao, X.; Zuo, Q.; Zhang, Z.; Han, D. Influence of geometric characteristics of a diesel particulate filter on its behavior in equilibrium state. *Appl. Therm. Eng.* **2017**, *123*, 61–73. [[CrossRef](#)]
55. Bai, S.-Z.; Tang, J.; Wang, G.-H.; Li, G.-X. Soot loading estimation model and passive regeneration characteristics of DPF system for heavy-duty engine. *Appl. Therm. Eng.* **2016**, *100*, 1292–1298. [[CrossRef](#)]
56. Meng, Z.; Chen, Z.; Tan, J.; Wang, W.; Zhang, Z.; Huang, J.; Fang, J. Regeneration performance and particulate emission characteristics during active regeneration process of GPF with ash loading. *Chem. Eng. Sci.* **2022**, *248*, 117114. [[CrossRef](#)]
57. Corro, G.; Pal, U.; Ayala, E.; Vidal, E. Diesel soot oxidation over silver-loaded SiO₂ catalysts. *Catal. Today* **2013**, *212*, 63–69. [[CrossRef](#)]
58. Gehrke, S.; Kovács, D.; Eilts, P.; Rempel, A.; Eckert, P. Investigation of VVA-based exhaust management strategies by means of a HD single cylinder research engine and rapid prototyping systems. *SAE Int. J. Commer. Veh.* **2013**, *6*, 47–61. [[CrossRef](#)]
59. Guan, W.; Zhao, H.; Ban, Z.; Lin, T. Exploring alternative combustion control strategies for low-load exhaust gas temperature management of a heavy-duty diesel engine. *Int. J. Engine Res.* **2019**, *20*, 381–392. [[CrossRef](#)]
60. Jiaqiang, E.; Liu, M.; Deng, Y.; Zhu, H.; Gong, J. Influence analysis of monolith structure on regeneration temperature in the process of microwave regeneration in the diesel particulate filter. *Can. J. Chem. Eng.* **2015**, *1*, 168–174.

61. Pallavkar, S.; Kim, T.-H.; Rutman, D.; Lin, J.; Ho, T. Active regeneration of diesel particulate filter employing microwave heating. *Ind. Eng. Chem. Res.* **2009**, *48*, 69–79. [[CrossRef](#)]
62. Chen, P.; Wangm, J. Control-oriented model for integrated diesel engine and after-treatment systems thermal management. *Control Eng. Pract.* **2014**, *22*, 81–93. [[CrossRef](#)]
63. Parks, J.; Huff, S.; Kass, M.; Storey, J. Characterization of in-cylinder techniques for thermal management of diesel after-treatment. In Proceedings of the Powertrain & Fluid Systems Conference and Exhibition, Rosemont, IL, USA, 29 October–1 November 2007.
64. Lee, D.H.; Kim, H.; Song, Y.H.; Kim, K.T. Plasma burner for active regeneration of diesel particulate filter. *Plasma Chem. Plasma Process.* **2014**, *34*, 159–173. [[CrossRef](#)]
65. Fang, X.; Mastbergen, D.; Paterson, C. Diesel particulate filter burner system modeling, control and diagnosis. In Proceedings of the Commercial Vehicle Engineering Congress, Rosemont, IL, USA, 13–14 September 2011.
66. Li, Z.; Cai, D.; He, L.; Cao, L.; Li, Z.; Meng, Y. NO₂-Assisted Regeneration Performance Enhancement of Catalyzed Diesel Particulate Filters. *Environ. Eng. Sci.* **2019**, *36*, 922–936. [[CrossRef](#)]
67. Jiaqiang, E.; Xie, L.; Zuo, Q.; Zhang, G. Effect analysis on regeneration speed of continuous regeneration-diesel particulate filter based on NO₂-assisted regeneration. *Atmos. Pollut. Res.* **2016**, *7*, 9–17.
68. Wu, G.; Li, Z.; Abubakar, S.; Li, Y.; Li, Y. Numerical study on effects of key factors on performance of CeO₂-based catalyzed diesel particulate filter. *J. Therm. Sci.* **2020**, *29*, 1398–1409. [[CrossRef](#)]
69. Li, Z.; Li, Y.; Liu, Z.; Wu, G.; Huang, J. Multi-objective optimization of composite regeneration performance of a CeO₂-based catalyzed diesel particulate filter. *Energy Sources Part A Recovery Util. Environ. Eff.* **2021**, 1–16. [[CrossRef](#)]
70. Zhao, X.; Jiaqiang, E.; Liao, G.; Zhang, F.; Chen, J.; Deng, Y. Numerical simulation study on soot continuous regeneration combustion model of diesel particulate filter under exhaust gas heavy load. *Fuel* **2021**, *290*, 119795. [[CrossRef](#)]
71. Chen, K.; Martirosyan, K.; Luss, D. Transient temperature rise during regeneration of diesel particulate filters. *Chem. Eng. J.* **2011**, *176*, 144–150. [[CrossRef](#)]
72. Zhang, B.; Jiaqiang, E.; Gong, J.; Yuan, W.; Zhao, X.; Hu, W. Influence of structural and operating factors on performance degradation of the diesel particulate filter based on composite regeneration. *Appl. Therm. Eng.* **2017**, *121*, 838–852. [[CrossRef](#)]
73. Wei, Y.; Liang, P.; Li, Y.; Zhao, Y.; Min, X.; Tao, P.; Hu, J.; Sun, T. Modification of Mn-Fe mixed oxide catalysts for low-temperature NH₃-SCR of NO from marine diesel exhausts. *J. Environ. Chem. Eng.* **2022**, *10*, 107772. [[CrossRef](#)]
74. Zhang, B.; Jiaqiang, E.; Gong, J.; Yuan, W.; Zuo, W.; Li, Y.; Fu, J. Multidisciplinary design optimization of the diesel particulate filter in the composite regeneration process. *Appl. Energy* **2016**, *181*, 14–28. [[CrossRef](#)]
75. Maunula, T. Intensification of catalytic after-treatments systems for mobile applications. In Proceedings of the SAE 2013 World Congress & Exhibition, Detroit, MI, USA, 16–18 April 2013.
76. Guan, B.; Zhan, R.; Lin, H.; Huang, Z. Review of state of the art technologies of selective catalytic reduction of NO_x from diesel engine exhaust. *Appl. Therm. Eng.* **2014**, *66*, 395–414. [[CrossRef](#)]
77. Shrestha, S.; Harold, M.P.; Kamasamudram, K.; Kumar, A.; Olsson, L.; Leistner, K. Selective oxidation of ammonia to nitrogen on bi-functional Cu-SSZ-13 and Pt/Al₂O₃ monolith catalyst. *Catal. Today* **2016**, *267*, 130–144. [[CrossRef](#)]
78. Maunula, T.; Tuikka, M.; Wolff, T. The reactions and role of ammonia slip catalysts in modern urea-SCR Systems. *Emiss. Control Sci. Technol.* **2020**, *6*, 390–401. [[CrossRef](#)]
79. Pârvolescu, V.I.; Grange, P.; Delmon, B. Catalytic removal of NO. *Catal. Today* **1998**, *46*, 233–316. [[CrossRef](#)]
80. Scheuer, A.; Hauptmann, W.; Drochner, A.; Gieshoff, J.; Vogel, H.; Votsmeier, M. Dual layer automotive ammonia oxidation catalysts: Experiments and computer simulation. *Appl. Catal. B Environ.* **2012**, *111*, 445–455. [[CrossRef](#)]
81. Zhang, H.; Wang, J. Adaptive sliding-mode observer design for a selective catalytic reduction system of ground-vehicle diesel engines. *IEEE/ASME Trans. Mechatron.* **2016**, *21*, 2027–2038. [[CrossRef](#)]
82. Roberts, L.; Magee, M.; Shaver, G.; Garg, A.; McCarthy, J.; Koeberlein, E.; Holloway, E.; Shute, R.; Koeberlein, D.; Nielsen, D. Modeling the impact of early exhaust valve opening on exhaust after-treatment thermal management and efficiency for compression ignition engines. *Int. J. Engine Res.* **2015**, *16*, 773–794. [[CrossRef](#)]
83. Basaran, H.U.; Ozsoysal, O.A. Effects of application of variable valve timing on the exhaust gas temperature improvement in a low-loaded diesel engine. *Appl. Therm. Eng.* **2017**, *122*, 758–767. [[CrossRef](#)]
84. Bai, S.; Chen, G.; Sun, Q.; Wang, G.; Li, G.-X. Influence of active control strategies on exhaust thermal management for diesel particulate filter active regeneration. *Appl. Therm. Eng.* **2017**, *119*, 297–303. [[CrossRef](#)]
85. Wu, B.; Jia, Z.; Li, Z.G.; Liu, G.Y.; Zhong, X.L. Different exhaust temperature management technologies for heavy-duty diesel engines with regard to thermal efficiency. *Appl. Therm. Eng.* **2021**, *186*, 116495. [[CrossRef](#)]
86. Xu, G.; Jia, M.; Li, Y.; Chang, Y.; Liu, H.; Wang, T. Evaluation of variable compression ratio (VCR) and variable valve timing (VVT) strategies in a heavy-duty diesel engine with reactivity controlled compression ignition (RCCI) combustion under a wide load range. *Fuel* **2019**, *253*, 114–128. [[CrossRef](#)]
87. Hong, H.; Parvate-Patil, G.B.; Gordon, B. Review and analysis of variable valve timing strategies—Eight ways to approach. *Proc. Inst. Mech. Eng. Part D J. Automob. Eng.* **2004**, *218*, 1179–1200. [[CrossRef](#)]
88. Zhao, X.; Jiang, J.; Zuo, H.; Mao, Z. Performance analysis of diesel particulate filter thermoelectric conversion mobile energy storage system under engine conditions of low-speed and light-load. *Energy* **2023**, *282*, 128411. [[CrossRef](#)]
89. Ho, P.H.; Woo, J.W.; Feizie Ilmasani, R.; Han, J.; Olsson, L. The role of Pd–Pt Interactions in the Oxidation and Sulfur Resistance of Bimetallic Pd–Pt/ γ -Al₂O₃ Diesel Oxidation Catalysts. *Ind. Eng. Chem. Res.* **2021**, *60*, 6596–6612. [[CrossRef](#)]

90. Farhan, S.M.; Wang, P. Post-injection strategies for performance improvement and emissions reduction in DI diesel engines—A review. *Fuel Process. Technol.* **2022**, *228*, 107145. [[CrossRef](#)]
91. Zhang, J.; Lou, D.; Sun, Y.; Tan, P.; Hu, Z.; Huang, C. Effects of DOC and CDPF catalyst composition on emission characteristics of light-duty diesel engine with DOC + CDPF + SCR system. In Proceedings of the WCX World Congress Experience, Detroit, MI, USA, 10–12 April 2018.
92. Garg, A.; Magee, M.; Ding, C.; Roberts, L.; Shaver, G.; Koeberlein, E.; Shute, R.; Koeberlein, D.; McCarthy, J.J.; Nielsen, D. Fuel-efficient exhaust thermal management using cylinder throttling via intake valve closing timing modulation. *Proc. Inst. Mech. Eng. Part D J. Automob. Eng.* **2016**, *230*, 470–478. [[CrossRef](#)]
93. Ding, C.; Roberts, L.; Fain, D.J.; Ramesh, A.K.; Shaver, G.M.; McCarthy, J.J.; Ruth, M.; Koeberlein, E.; Holloway, E.A.; Nielsen, D. Fuel efficient exhaust thermal management for compression ignition engines during idle via cylinder deactivation and flexible valve actuation. *Int. J. Engine Res.* **2016**, *17*, 619–630. [[CrossRef](#)]
94. Neely, G.D.; Sarlashkar, J.V.; Mehta, D. Diesel cold-start emission control research for 2015–2025 LEV III emissions. *SAE Int. J. Engines* **2013**, *6*, 1009–1020. [[CrossRef](#)]
95. Arnau, F.J.; Martín, J.; Piqueras, P.; Auñón, Á. Effect of the exhaust thermal insulation on the engine efficiency and the exhaust temperature under transient conditions. *Int. J. Engine Res.* **2021**, *22*, 2869–2883. [[CrossRef](#)]
96. Zhao, Z.; Zheng, G.; Shan, X.; Kotrba, A.J. CFD modeling of mini and full flow burner systems for diesel engine after-treatment under low temperature conditions. In Proceedings of the SAE 2012 Commercial Vehicle Engineering Congress, Rosemont, IL, USA, 2–3 October 2012.
97. Ferreri, P.; Cerrelli, G.; Miao, Y.; Pellegrino, S.; Bianchi, L. Conventional and electrically heated diesel oxidation catalyst physical based modeling. In Proceedings of the CO₂ Reduction for Transportation Systems Conference, Turin, Italy, 7–8 July 2018.
98. Chen, K.; Martirosyan, K.; Luss, D. Temperature gradients within a soot layer during DPF regeneration. *Chem. Eng. Sci.* **2011**, *66*, 2968–2973. [[CrossRef](#)]
99. Castoldi, L.; Matarrese, R.; Lietti, L.; Forzatti, P. Intrinsic reactivity of alkaline and alkaline-earth metal oxide catalysts for oxidation of soot. *Appl. Catal. B Environ.* **2009**, *90*, 278–285. [[CrossRef](#)]
100. Zhang, Z.; Dong, R.; Lan, G.; Yuan, T.; Tan, D. Diesel particulate filter regeneration mechanism of modern automobile engines and methods of reducing PM emissions: A review. *Environ. Sci. Pollut. Res.* **2023**, *30*, 39338–39376. [[CrossRef](#)]
101. Meng, Z.; Wang, W.; Zeng, B.; Bao, Z.; Hu, Y.; Ou, J.; Liu, J. An experimental investigation of particulate emission characteristics of catalytic diesel particulate filters during passive regeneration. *Chem. Eng. J.* **2023**, *468*, 143549. [[CrossRef](#)]
102. Tan, P.; Duan, L.; Li, E.; Hu, Z.; Lou, D. Experimental Study on Thermal Management Strategy of the Exhaust Gas of a Heavy-Duty Diesel Engine Based on In-Cylinder Injection Parameters. In Proceedings of the WCX SAE World Congress Experience, Detroit, MI, USA, 21–23 April 2020.
103. Yoon, S.; Kim, H.; Kim, D.; Park, S. Effect of the fuel injection strategy on diesel particulate filter regeneration in a single-cylinder diesel engine. *J. Eng. Gas Turbines Power* **2016**, *138*, 102810. [[CrossRef](#)]
104. Chiew, L.; Kroner, P.; Ranalli, M. Diesel vaporizer: An innovative technology for reducing complexity and costs associated with DPF regeneration. In Proceedings of the SAE 2005 World Congress & Exhibition, Detroit, MI, USA, 11–14 April 2005.
105. Gardner, T.; Yetkin, A.; Shotwell, R.; Kotrba, A.; Gysling, H.; Mustafa, Z.; Holroyd, J. Evaluation of a DPF regeneration system and DOC performance using secondary fuel injection. In Proceedings of the SAE 2009 Commercial Vehicle Engineering Congress & Exhibition, Rosemont, IL, USA, 6–7 October 2009.
106. Kurien, C.; Srivastava, A.K.; Gandigudi, N.; Anand, K. Soot deposition effects and microwave regeneration modelling of diesel particulate filtration system. *J. Energy Inst.* **2020**, *93*, 463–473. [[CrossRef](#)]
107. Jiaqiang, E.; Zhao, X.; Liu, G.; Zhang, B.; Zuo, Q.; Wei, K.; Li, H.; Han, D.; Gong, J. Effects analysis on optimal microwave energy consumption in the heating process of composite regeneration for the diesel particulate filter. *Appl. Energy* **2019**, *254*, 113736.
108. Jiaqiang, E.; Zhao, M.; Zuo, Q.; Zhang, B.; Zhang, Z.; Peng, Q.; Dan, H.; Zhao, X.; Deng, Y. Effects analysis on diesel soot continuous regeneration performance of a rotary microwave-assisted regeneration diesel particulate filter. *Fuel* **2020**, *260*, 116353.
109. Jiaqiang, E.; Zheng, P.; Han, D.; Zhao, X.; Deng, Y. Effects analysis on soot combustion performance enhancement in a rotary diesel particulate filter unit during continuous microwave heating. *Fuel* **2020**, *276*, 118043.
110. Zhao, X.; Jiaqiang, E.; Zhang, Z.; Chen, J.; Liao, G.; Zhang, F.; Leng, E.; Han, D.; Hu, W. A review on heat enhancement in thermal energy conversion and management using Field Synergy Principle. *Appl. Energy* **2020**, *257*, 113995. [[CrossRef](#)]
111. Deng, Y.; Cui, J.; Jiaqiang, E.; Zhang, B.; Zhao, X.; Zhang, Z.; Han, D. Investigations on the temperature distribution of the diesel particulate filter in the thermal regeneration process and its field synergy analysis. *Appl. Therm. Eng.* **2017**, *123*, 92–102. [[CrossRef](#)]
112. Jiaqiang, E.; Zhao, X.; Xie, L.; Zhang, B.; Chen, J.; Zuo, Q.; Han, D.; Hu, W.; Zhang, Z. Performance enhancement of microwave assisted regeneration in a wall-flow diesel particulate filter based on field synergy theory. *Energy* **2019**, *169*, 719–729. [[CrossRef](#)]
113. Shankar, R.; Chauhan, A.; Krishnan, N.; Chandrasekaran, V. Investigation of Temperature Distribution inside the Diesel Particulate Filter (DPF) during the Drop to Idle Test (DTIT) Performed at Steady-State and Worst-Case Driving Cycles. In Proceedings of the SAE WCX Digital Summit, Online, 12–15 April 2021.
114. Lee, K.-B.; Kim, S.-H.; Oh, K.C. The effect of pore structure on thermal characteristics of a cordierite diesel particulate filter for heavy duty diesel vehicle. *Int. J. Automot. Technol.* **2021**, *22*, 243–251. [[CrossRef](#)]
115. Merkel, G.A.; Cutler, W.A.; Warren, C.J. Thermal durability of wall-flow ceramic diesel particulate filters. In Proceedings of the SAE 2001 World Congress, Detroit, MI, USA, 5–8 March 2001.

116. Chen, K.; Luss, D. Temperature rise during stationary and dynamic regeneration of a diesel particulate filter. *Rev. Chem. Eng.* **2010**, *26*, 133–147. [[CrossRef](#)]
117. Wang, D.; Liu, Z.C.; Tian, J. Control strategies for safe diesel particulate filter uncontrolled regeneration during idle. *Adv. Mater. Res.* **2013**, *614*, 366–370. [[CrossRef](#)]
118. Bai, S.; Wang, C.; Li, D.; Wang, G.; Li, G. Influence of the idle-up strategy on the thermal management of diesel particulate filter regeneration during a drop to the idle process. *Appl. Therm. Eng.* **2018**, *141*, 976–980. [[CrossRef](#)]
119. Tan, P.-Q.; Duan, L.-S.; Li, E.-F.; Hu, Z.-Y.; Lou, D.-M. Experimental study on the temperature characteristics of a diesel particulate filter during a drop to idle active regeneration process. *Appl. Therm. Eng.* **2020**, *178*, 115628. [[CrossRef](#)]
120. Liu, F.; He, H.; Zhang, C.; Feng, Z.; Zheng, L.; Xie, Y.; Hu, T. Selective catalytic reduction of NO with NH₃ over iron titanate catalyst: Catalytic performance and characterization. *Appl. Catal. B Environ.* **2010**, *96*, 408–420. [[CrossRef](#)]
121. Cavina, N.; Mancini, G.; Corti, E.; Moro, D.; De Cesare, M.; Stola, F. Thermal management strategies for SCR after treatment systems. In Proceedings of the 11th International Conference on Engines & Vehicles, Napoli, Italy, 15–19 September 2013.
122. Pyun, S.H.; Lee, D.H.; Kim, K.T. Development of a unique plasma burner system for emission reduction during cold start of diesel engines. In Proceedings of the SAE 2014 World Congress & Exhibition, Detroit, MI, USA, 8–10 April 2014.
123. Culbertson, D.; Khair, M.; Zhang, S.; Tan, J.; Spooler, J. The study of exhaust heating to improve SCR cold start performance. *SAE Int. J. Engines* **2015**, *8*, 1187–1195. [[CrossRef](#)]
124. Nova, I.; Ciardelli, C.; Tronconi, E.; Chatterjee, D.; Bandl-Konrad, B. NH₃-NO/NO₂ chemistry over V-based catalysts and its role in the mechanism of the Fast SCR reaction. *Catal. Today* **2006**, *114*, 3–12. [[CrossRef](#)]
125. Zhang, X.J.; Zhang, T.J.; Song, Z.X.; Liu, W.; Xing, Y. Effect of sulfate species on the performance of Ce-Fe-O_x catalysts in the selective catalytic reduction of NO by NH₃. *J. Fuel Chem. Technol.* **2021**, *49*, 844–852. [[CrossRef](#)]
126. Kwak, J.H.; Tran, D.; Burton, S.D.; Szanyi, J.; Lee, J.H.; Peden, C.H. Effects of hydrothermal aging on NH₃-SCR reaction over Cu/zeolites. *J. Catal.* **2012**, *287*, 203–209. [[CrossRef](#)]
127. Shan, Y.; Sun, Y.; Du, J.; Zhang, Y.; Shi, X.; Yu, Y.; Shan, W.; He, H. Hydrothermal aging alleviates the inhibition effects of NO₂ on Cu-SSZ-13 for NH₃-SCR. *Appl. Catal. B Environ.* **2020**, *275*, 119105. [[CrossRef](#)]
128. Harris, T. Simulation of After-treatment Thermal Management Strategies for Low-Load Operation. In Proceedings of the WCX SAE World Congress Experience, Detroit, MI, USA, 21–23 April 2020.
129. Jiang, J.; Li, D. Theoretical analysis and experimental confirmation of exhaust temperature control for diesel vehicle NO_x emissions reduction. *Appl. Energy* **2016**, *174*, 232–244. [[CrossRef](#)]
130. zu Schweinsberg, A.S.; Klenk, M.; Degen, A. Engine-independent exhaust gas after-treatment using a burner heated catalyst. In Proceedings of the Powertrain & Fluid Systems Conference and Exhibition, Toronto, ON, Canada, 16–19 October 2006.
131. Harris, T.M.; Gardner, T. Modeling of After-treatment Technologies to Meet a Future HD Low-NO_x Standard. In Proceedings of the International Powertrains, Fuels & Lubricants Meeting, Kyoto, Japan, 26–29 August 2019.
132. Harris, T.; Bellard, R.; Muhleck, M.; Palmer, G. Pre-Heating the After-treatment System with a Burner. In Proceedings of the WCX SAE World Congress Experience, Detroit, MI, USA, 5–7 April 2022.
133. McCarthy, J., Jr.; Matheaus, A.; Zavala, B.; Sharp, C.; Harris, T. Meeting Future NO_x Emissions Over Various Cycles Using a Fuel Burner and Conventional After-treatment System. In Proceedings of the WCX SAE World Congress Experience, Detroit, MI, USA, 5–7 April 2022.
134. Della Torre, A.; Montenegro, G.; Onorati, A.; Cerri, T. CFD Investigation of the Impact of Electrical Heating on the Light-off of a Diesel Oxidation Catalyst. In Proceedings of the WCX World Congress Experience, Detroit, MI, USA, 10–12 April 2018.
135. Hofstetter, J.; Boucharel, P.; Atzler, F.; Wachtmeister, G. Fuel consumption and emission reduction for hybrid electric vehicles with electrically heated catalyst. *SAE Int. J. Adv. Curr. Pract. Mobil.* **2020**, *3*, 702–714. [[CrossRef](#)]
136. Pfahl, U.; Schatz, A.; Konieczny, R. Advanced exhaust gas thermal management for lowest tailpipe emissions-combining low emission engine and electrically heated catalyst. In Proceedings of the SAE 2012 World Congress & Exhibition, Detroit, MI, USA, 24–26 April 2012.
137. Pace, L.; Presti, M. An alternative way to reduce fuel consumption during cold start: The electrically heated catalyst. In Proceedings of the 10th International Conference on Engines & Vehicles, Naples, Italy, 10–14 September 2023.
138. Gao, J.; Tian, G.; Sornioti, A. On the emission reduction through the application of an electrically heated catalyst to a diesel vehicle. *Energy Sci. Eng.* **2019**, *7*, 2383–2397. [[CrossRef](#)]
139. Hamed, M.R.; Doustdar, O.; Tsolakis, A.; Hartland, J. Energy-efficient heating strategies of diesel oxidation catalyst for low emissions vehicles. *Energy* **2021**, *230*, 120819. [[CrossRef](#)]
140. Bargman, B.; Jang, S.; Kramer, J.; Soliman, I.; Sahul, A.A.A.M. Effects of Electrically Preheating Catalysts on Reducing High-Power Cold-Start Emissions. In Proceedings of the SAE WCX Digital Summit, Online, 12–15 April 2021.
141. Kim, C.H.; Paratore, M.; Gonze, E.; Solbrig, C.; Smith, S. Electrically heated catalysts for cold-start emissions in diesel after-treatment. In Proceedings of the SAE 2012 World Congress & Exhibition, Detroit, MI, USA, 24–26 April 2012.
142. Matheaus, A.; Neely, G.; Sharp, C.; Hopkins, J.; McCarthy, J., Jr. Fast Diesel After-treatment Heat-up Using CDA and an Electrical Heater. In Proceedings of the SAE WCX Digital Summit, Online, 12–15 April 2021.
143. Massaguer, A.; Pujol, T.; Comamala, M.; Massaguer, E. Feasibility study on a vehicular thermoelectric generator coupled to an exhaust gas heater to improve after-treatment's efficiency in cold-starts. *Appl. Therm. Eng.* **2020**, *167*, 114702. [[CrossRef](#)]

144. Ximinis, J.; Massaguer, A.; Pujol, T.; Massaguer, E. Nox emissions reduction analysis in a diesel Euro VI Heavy Duty vehicle using a thermoelectric generator and an exhaust heater. *Fuel* **2021**, *301*, 121029. [[CrossRef](#)]
145. Broatch, A.; Olmeda, P.; Martin, J.; Dreif, A. Numerical Study of the Maximum Impact on Engine Efficiency When Insulating the Engine Exhaust Manifold and Ports during Steady and Transient Conditions. *SAE Int. J. Adv. Curr. Pract. Mobil.* **2020**, *3*, 661–671. [[CrossRef](#)]
146. Daya, R.; Hoard, J.; Chanda, S.; Singh, M. Insulated catalyst with heat storage for real-world vehicle emissions reduction. *Int. J. Engine Res.* **2017**, *18*, 886–899. [[CrossRef](#)]
147. Wang, T.J. Effects of insulation on exhaust temperature and subsequent SCR efficiency of a heavy-duty diesel engine. *J. Mech. Sci. Technol.* **2019**, *33*, 923–929. [[CrossRef](#)]
148. Wang, Y.; Ma, T.; Liu, L.; Yao, M. Numerical investigation of the effect of thermal barrier coating on combustion and emissions in a diesel engine. *Appl. Therm. Eng.* **2021**, *186*, 116497. [[CrossRef](#)]
149. Luján, J.M.; Serrano, J.R.; Piqueras, P.; Diesel, B. Turbine and exhaust ports thermal insulation impact on the engine efficiency and after-treatment inlet temperature. *Appl. Energy* **2019**, *240*, 409–423. [[CrossRef](#)]
150. Riffat, S.; Mempo, B.; Fang, W. Phase change material developments: A review. *Int. J. Ambient. Energy* **2015**, *36*, 102–115. [[CrossRef](#)]
151. Pielichowska, K.; Pielichowski, K. Phase change materials for thermal energy storage. *Prog. Mater. Sci.* **2014**, *65*, 67–123. [[CrossRef](#)]
152. Jankowski, N.R.; McCluskey, F.P. A review of phase change materials for vehicle component thermal buffering. *Appl. Energy* **2014**, *113*, 1525–1561. [[CrossRef](#)]
153. Jaguemont, J.; Omar, N.; Van den Bossche, P.; Mierlo, J. Phase-change materials (PCM) for automotive applications: A review. *Appl. Therm. Eng.* **2018**, *132*, 308–320. [[CrossRef](#)]
154. Korin, E.; Reshef, R.; Tshernichovesky, D.; Sher, E. Reducing cold-start emission from internal combustion engines by means of a catalytic converter embedded in a phase-change material. *Proc. Inst. Mech. Eng. Part D J. Automob. Eng.* **1999**, *213*, 575–583. [[CrossRef](#)]
155. Gaiser, G.; Seethaler, C. Zero-Delay Light-Off-A New Cold-Start Concept with a Latent Heat Storage Integrated into a Catalyst Substrate. In Proceedings of the SAE World Congress & Exhibition, Detroit, MI, USA, 16–19 April 2007.
156. Hamedi, M.R.; Doustdar, O.; Tsolakis, A.; Hartland, J. Thermal energy storage system for efficient diesel exhaust after-treatment at low temperatures. *Appl. Energy* **2019**, *235*, 874–887. [[CrossRef](#)]
157. Raznoshinskaia, A.; Troyanovskaya, I.; Kozminykh, V. Heat-storing phase-change materials: Influence of thermophysical properties on stabilization of exhaust temperature. *Mater. Today Proc.* **2019**, *19*, 1831–1834. [[CrossRef](#)]
158. Lee, D.H.; Lee, J.S.; Park, J.S. Effects of secondary combustion on efficiencies and emission reduction in the diesel engine exhaust heat recovery system. *Appl. Energy* **2010**, *87*, 1716–1721. [[CrossRef](#)]
159. Park, S.; Woo, S.; Shon, J.; Lee, K. Numerical model and simulation of a vehicular heat storage system with phase-change material. *Appl. Therm. Eng.* **2017**, *113*, 1496–1504. [[CrossRef](#)]
160. Gumus, M.; Ugurlu, A. Application of phase change materials to pre-heating of evaporator and pressure regulator of a gaseous sequential injection system. *Appl. Energy* **2011**, *88*, 4803–4810. [[CrossRef](#)]
161. Arnau, F.J.; Martín, J.; Pla, B.; Auñón, Á. Diesel engine optimization and exhaust thermal management by means of variable valve train strategies. *Int. J. Engine Res.* **2021**, *22*, 1196–1213. [[CrossRef](#)]
162. Zhao, J.; Xi, Q.; Wang, S.; Wang, S. Improving the partial-load fuel economy of 4-cylinder SI engines by combining variable valve timing and cylinder-deactivation through double intake manifolds. *Appl. Therm. Eng.* **2018**, *141*, 245–256. [[CrossRef](#)]
163. Said, M.F.M.; Aziz, A.B.A.; Latiff, Z.A.; Andwari, A.M.; Soid, S.N.M. Investigation of cylinder deactivation (CDA) strategies on part load conditions. In Proceedings of the SAE 2014 International Powertrain, Fuels & Lubricants Meeting, Birmingham, UK, 20–22 October 2014.
164. Fridrichová, K.; Drápal, L.; Vopařil, J.; Dluhoš, J. Overview of the potential and limitations of cylinder deactivation. *Renew. Sustain. Energy Rev.* **2021**, *146*, 111196. [[CrossRef](#)]
165. Zammit, J.; McGhee, M.; Shayler, P.; Law, T.; Pegg, I. The effects of early inlet valve closing and cylinder disablement on fuel economy and emissions of a direct injection diesel engine. *Energy* **2015**, *79*, 100–110. [[CrossRef](#)]
166. Pillai, S.; LoRusso, J.; Van Benschoten, M. Analytical and experimental evaluation of cylinder deactivation on a diesel engine. In Proceedings of the SAE 2015 Commercial Vehicle Engineering Congress, Rosemont, IL, USA, 6–8 October 2015.
167. Ramesh, A.K.; Gosala, D.B.; Allen, C.; Joshi, M.; McCarthy, J., Jr.; Farrell, L.; Koeberlein, E.D.; Shaver, G. Cylinder deactivation for increased engine efficiency and after-treatment thermal management in diesel engines. In Proceedings of the WCX World Congress Experience, Detroit, MI, USA, 10–12 April 2018.
168. Allen, C.M.; Joshi, M.C.; Gosala, D.B.; Shaver, G.M.; Farrell, L.; McCarthy, J. Experimental assessment of diesel engine cylinder deactivation performance during low-load transient operations. *Int. J. Engine Res.* **2021**, *22*, 606–615. [[CrossRef](#)]
169. Joshi, M.C.; Shaver, G.M.; Vos, K.; McCarthy, J., Jr.; Farrell, L. Internal exhaust gas recirculation via reinduction and negative valve overlap for fuel-efficient after-treatment thermal management at curb idle in a diesel engine. *Int. J. Engine Res.* **2022**, *23*, 369–379. [[CrossRef](#)]
170. Joshi, M.C.; Gosala, D.; Shaver, G.M.; McCarthy, J.; Farrell, L. Exhaust valve profile modulation for improved diesel engine curb idle after-treatment thermal management. *Int. J. Engine Res.* **2021**, *22*, 3179–3195. [[CrossRef](#)]

171. Wang, Z.; Shen, L.; Lei, J.; Yao, G.; Wang, G. Impact characteristics of post injection on exhaust temperature and hydrocarbon emissions of a diesel engine. *Energy Rep.* **2022**, *8*, 4332–4343. [[CrossRef](#)]
172. Huang, T.; Hu, G.; Meng, Z.; Zeng, D. Exhaust temperature control for safe and efficient thermal regeneration of diesel particulate filter. *Appl. Therm. Eng.* **2021**, *189*, 116747. [[CrossRef](#)]
173. Andersson, J.; Antonsson, M.; Eurenus, L.; Olsson, E.; Skoglundh, M. Deactivation of diesel oxidation catalysts: Vehicle-and synthetic aging correlations. *Appl. Catal. B Environ.* **2007**, *72*, 71–81. [[CrossRef](#)]
174. Abedi, A.; Luo, J.-Y.; Epling, W.S. Improved CO, hydrocarbon and NO oxidation performance using zone-coated Pt-based catalysts. *Catal. Today* **2013**, *207*, 220–226. [[CrossRef](#)]
175. Kolli, T.; Kanerva, T.; Huuhtanen, M.; Vippola, M.; Kallinen, K.; Kinnunen, T.; Lepistö, T.; Lahtinen, J.; Keiski, R.L. The activity of Pt/Al₂O₃ diesel oxidation catalyst after sulphur and calcium treatments. *Catal. Today* **2010**, *154*, 303–307. [[CrossRef](#)]
176. Boubnov, A.; Dahl, S.; Johnson, E.; Molina, A.P.; Simonsen, S.B.; Cano, F.M.; Helveg, S.; Lemus-Yegres, L.J.; Grunwaldt, J.-D. Structure–activity relationships of Pt/Al₂O₃ catalysts for CO and NO oxidation at diesel exhaust conditions. *Appl. Catal. B Environ.* **2012**, *126*, 315–325. [[CrossRef](#)]
177. Liang, Y.; Zhao, B.; Wang, J.; Zhao, M.; Cheng, Y. Enhanced performance of Pt-based diesel oxidation catalyst via defective MnO_x: The role of Pt/MnO_x interface. *Mol. Catal.* **2022**, *521*, 112198. [[CrossRef](#)]
178. Väliheikki, A.; Kärkkäinen, M.; Honkanen, M.; Heikkinen, O.; Kolli, T.; Kallinen, K.; Huuhtanen, M.; Vippola, M.; Lahtinen, J.; Keiski, R.L. Deactivation of Pt/SiO₂-ZrO₂ diesel oxidation catalysts by sulphur, phosphorus and their combinations. *Appl. Catal. B Environ.* **2017**, *218*, 409–419. [[CrossRef](#)]
179. Gu, L.; Chen, X.; Zhou, Y.; Zhu, Q.; Huang, H.; Lu, H. Propene and CO oxidation on Pt/Ce-Zr-SO₄²⁻ diesel oxidation catalysts: Effect of sulfate on activity and stability. *Chin. J. Catal.* **2017**, *38*, 607–615. [[CrossRef](#)]
180. Liang, Y.; Zhao, M.; Wang, J.; Sun, M.; Li, S.; Huang, Y.; Zhong, L.; Gong, M.; Chen, Y. Enhanced activity and stability of the monolithic Pt/SiO₂-Al₂O₃ diesel oxidation catalyst promoted by suitable tungsten additive amount. *J. Ind. Eng. Chem.* **2017**, *54*, 359–368. [[CrossRef](#)]
181. Kim, C.H.; Schmid, M.; Schmiege, S.J.; Tan, J.; Li, W. The effect of Pt-Pd ratio on oxidation catalysts under simulated diesel exhaust. In Proceedings of the SAE 2011 World Congress & Exhibition, Detroit, MI, USA, 12–14 April 2011.
182. Huang, H.; Jiang, B.; Gu, L.; Qi, Z.; Lu, H. Promoting effect of vanadium on catalytic activity of Pt/Ce-Zr-O diesel oxidation catalysts. *J. Environ. Sci.* **2015**, *33*, 135–142. [[CrossRef](#)]
183. Dong, F.; Yamazaki, K. The Pt-Pd alloy catalyst and enhanced catalytic activity for diesel oxidation. *Catal. Today* **2021**, *376*, 47–54. [[CrossRef](#)]
184. Franken, T.; Vieweger, E.; Klimera, A.; Hug, M.; Heel, A. Sulphur tolerant diesel oxidation catalysts by noble metal alloying. *Catal. Commun.* **2019**, *129*, 105732. [[CrossRef](#)]
185. O'Donnell, R. The Development of Ceria-Based Catalysts for Automotive After-Treatment Applications. Ph.D. Thesis, Queen's University of Belfast, Belfast, UK, 2021.
186. Di Sarli, V.; Landi, G.; Lisi, L.; Di Benedetto, A. Ceria-coated diesel particulate filters for continuous regeneration. *AIChE J.* **2017**, *63*, 3442–3449. [[CrossRef](#)]
187. Bueno-López, A. Diesel soot combustion ceria catalysts. *Appl. Catal. B Environ.* **2014**, *146*, 1–11. [[CrossRef](#)]
188. Liu, S.; Wu, X.; Weng, D.; Ran, R. Ceria-based catalysts for soot oxidation: A review. *J. Rare Earths* **2015**, *33*, 567–590. [[CrossRef](#)]
189. Yang, Z.; Zhang, N.; Xu, H.; Li, Y.; Ren, L.; Liao, Y.; Chen, Y. Boosting diesel soot catalytic combustion via enhancement of solid (catalyst)-solid (soot) contact by tailoring micrometer scaled sheet-type agglomerations of CeO₂-ZrO₂ catalyst. *Combust. Flame* **2022**, *235*, 111700. [[CrossRef](#)]
190. Song, C.; Jung, J.; Song, S.; Chun, K.M. Experimental study on soot oxidation characterization of Pt/CeO₂ catalyst with NO and O₂ using a flow reactor system. In Proceedings of the SAE World Congress & Exhibition, Detroit, MI, USA, 20–23 April 2009.
191. Pérez, V.R.; Bueno-López, A. Catalytic regeneration of diesel particulate filters: Comparison of Pt and CePr active phases. *Chem. Eng. J.* **2015**, *279*, 79–85. [[CrossRef](#)]
192. Quiles-Díaz, S.; Giménez-Mañogil, J.; García-García, A. Catalytic performance of CuO/Ce_{0.8}Zr_{0.2}O₂ loaded onto SiC-DPF in NO_x-assisted combustion of diesel soot. *RSC Adv.* **2015**, *5*, 17018–17029. [[CrossRef](#)]
193. Wu, X.; Hyeong-Ryeol, L.E.E.; Liu, S.; Weng, D. Sulfur poisoning and regeneration of MnO_x-CeO₂-Al₂O₃ catalyst for soot oxidation. *J. Rare Earths* **2012**, *30*, 659–664. [[CrossRef](#)]
194. Peralta, M.A.; Milt, V.G.; Cornaglia, L.M.; Querini, C.A. Stability of Ba, K/CeO₂ catalyst during diesel soot combustion: Effect of temperature, water, and sulfur dioxide. *J. Catal.* **2006**, *242*, 118–130. [[CrossRef](#)]
195. Neyertz, C.; Miró, E.; Querini, C. K/CeO₂ catalysts supported on cordierite monoliths: Diesel soot combustion study. *Chem. Eng. J.* **2012**, *181*, 93–102. [[CrossRef](#)]
196. Olong, N.E.; Stöwe, K.; Maier, W.F. A combinatorial approach for the discovery of low temperature soot oxidation catalysts. *Appl. Catal. B Environ.* **2007**, *74*, 19–25. [[CrossRef](#)]
197. Yang, Y.; Fang, J.; Meng, Z.; Pu, P.; Zhang, Q.; Yi, C.; Pan, S.; Li, Y. Catalytic activity and influence factors of Mn-Ce mixed oxides by hydrothermal method on diesel soot combustion. *Mol. Catal.* **2022**, *524*, 112334. [[CrossRef](#)]
198. Atribak, I.; Bueno-López, A.; García-García, A. Thermally stable ceria-zirconia catalysts for soot oxidation by O₂. *Catal. Commun.* **2008**, *9*, 250–255. [[CrossRef](#)]

199. Yang, Y.; Yang, Z.Z.; Xu, H.D.; Xu, B.Q.; Zhang, Y.H.; Gong, M.C.; Chen, Y.Q. Influence of La on CeO₂-ZrO₂ catalyst for oxidation of soluble organic fraction from diesel exhaust. *Acta Phys.-Chim. Sin.* **2015**, *31*, 2358–2365. [[CrossRef](#)]
200. Wu, G.; Tang, K.; Wu, D.; Li, Y.; Li, Y. Experimental evaluation on the catalytic activity of a novel CeZrK/rGO nanocomposite for soot oxidation in catalyzed diesel particulate filter. *Processes* **2021**, *9*, 674. [[CrossRef](#)]
201. Di Sarli, V.; Landi, G.; Di Benedetto, A.; Lisi, L. Synergy between ceria and metals (Ag or Cu) in catalytic diesel particulate filters: Effect of the metal content and of the preparation method on the regeneration performance. *Top. Catal.* **2021**, *64*, 256–269. [[CrossRef](#)]
202. Cheng, J.; Li, W.; Wang, X.; Liu, H.; Chen, Y. Vanadium-based catalytic fibers for selective reduction of NO by NH₃ and their potential use on co-processing of dust and NO_x. *Chem. Eng. J.* **2022**, *431*, 133694. [[CrossRef](#)]
203. Ding, S.; Li, C.; Bian, C.; Zhang, J.; Xu, Y.; Qian, G. Application of low-cost MFe₂O₄ (M = Cu, Mn, and Zn) spinels in low-temperature selective catalytic reduction of nitrogen oxide. *J. Clean. Prod.* **2022**, *330*, 129825. [[CrossRef](#)]
204. Zhang, Z.; Li, J.; Tian, J.; Zhong, Y.; Zou, Z.; Dong, R.; Gao, S.; Xu, W.; Tan, D. The effects of Mn-based catalysts on the selective catalytic reduction of NO_x with NH₃ at low temperature: A review. *Fuel Process. Technol.* **2022**, *230*, 107213. [[CrossRef](#)]
205. Tang, L.; Zhao, Z.; Li, K.; Yu, X.; Wei, Y.; Liu, J.; Peng, Y.; Li, Y.; Chen, Y. Highly active monolith catalysts of LaKCoO₃ perovskite-type complex oxide on alumina-wash coated diesel particulate filter and the catalytic performances for the combustion of soot. *Catal. Today* **2020**, *339*, 159–173. [[CrossRef](#)]
206. Zhao, D. Transient growth of flow disturbances in triggering a Rijke tube combustion instability. *Combust. Flame* **2012**, *159*, 2126–2137. [[CrossRef](#)]
207. Zhao, D.; Guan, Y.; Reinecke, A. Characterizing Hydrogen-fuelled pulsating combustion on thermodynamic properties of a combustor. *Commun. Phys.* **2019**, *2*, 44. [[CrossRef](#)]
208. Li, Y.; Tang, W.; Chen, Y.; Liu, J.; Lee, C.-F.F. Potential of acetone-butanol-ethanol (ABE) as a biofuel. *Fuel* **2019**, *242*, 673–686. [[CrossRef](#)]
209. Li, Y.; Chen, Y.; Wu, G.; Chia-fon, F.L.; Liu, J. Experimental comparison of acetone-n-butanol-ethanol (ABE) and isopropanol-n-butanol-ethanol (IBE) as fuel candidate in spark-ignition engine. *Appl. Therm. Eng.* **2018**, *133*, 179–187. [[CrossRef](#)]
210. Zhao, X.; Jiaqiang, E.; Wu, G.; Deng, Y.; Han, D.; Zhang, B.; Zhang, Z. A review of studies using graphenes in energy conversion, energy storage and heat transfer development. *Energy Convers. Manag.* **2019**, *184*, 581–599. [[CrossRef](#)]
211. Zhao, X.; Liu, F.; Wang, C. Effects of different piston combustion chamber heights on heat transfer and energy conversion performance enhancement of a heavy-duty truck diesel engine. *Energy* **2022**, *249*, 23732. [[CrossRef](#)]
212. Li, Y.; Chen, Y.; Wu, G.; Liu, J. Experimental evaluation of water-containing isopropanol-n-butanol-ethanol and gasoline blend as a fuel candidate in spark-ignition engine. *Appl. Energy* **2018**, *219*, 42–52. [[CrossRef](#)]
213. Wu, G.; Lu, Z.; Pan, W.; Guan, Y.; Li, S.; Ji, C.Z. Experimental demonstration of mitigating self-excited combustion oscillations using an electrical heater. *Appl. Energy* **2019**, *239*, 331–342. [[CrossRef](#)]
214. Zhao, X.; Zuo, H.; Jia, G. Effect analysis on pressure sensitivity performance of diesel particulate filter for heavy-duty truck diesel engine by the nonlinear soot regeneration combustion pressure model. *Energy* **2022**, *257*, 124766. [[CrossRef](#)]
215. Zhao, X.; Zuo, H.; Jia, G. Effects of the continuous pulsation regeneration on the soot combustion in diesel particulate filter for heavy-duty truck. *Chemosphere* **2022**, *306*, 135651. [[CrossRef](#)]
216. Zhao, X.; Jiang, J.; Mao, Z. Effect of filter material and porosity on the energy storage capacity characteristics of diesel particulate filter thermoelectric conversion mobile energy storage system. *Energy* **2023**, *283*, 129068. [[CrossRef](#)]
217. Ye, S.; Yap, Y.H.; Kolaczowski, S.T.; Robinson, K.; Lukyanov, D. Catalyst ‘light-off’ experiments on a diesel oxidation catalyst connected to a diesel engine-Methodology and techniques. *Chem. Eng. Res. Des.* **2012**, *90*, 834–845. [[CrossRef](#)]

Disclaimer/Publisher’s Note: The statements, opinions and data contained in all publications are solely those of the individual author(s) and contributor(s) and not of MDPI and/or the editor(s). MDPI and/or the editor(s) disclaim responsibility for any injury to people or property resulting from any ideas, methods, instructions or products referred to in the content.